Deep–Inelastic Physics with H1 at the HERA *ep* Collider

John B. Dainton

Oliver Lodge Laboratory, Department of Physics, The University of Liverpool, UK

for the H1 collaboration

Abstract

Recent measurements by the H1 experiment at HERA of deep–inelastic photon–proton (γp) and electron–proton (ep) scattering are presented. Their interpretation in terms of the partonic structure of the photon, proton, and diffractive exchange (sometimes understood as the pomeron) is emphasised.

1. Introduction: *ep* Physics and H1 1992 – 94

The H1 experiment [1] at the HERA ep collider at DESY, Hamburg, is an hermetic detector which has operated taking data since the start–up of HERA, the first electron–proton (ep) collider, in summer 1992 (figure 1 shows graphics displays of two ep DIS interactions). It is optimised for efficient and accurate measurements of ep physics in an environment in which an 820 GeV proton (p) beam (always from the right in any event graphics presented here) is incident head–on with a 27.6 GeV electron or positron (e) beam (always from the left). This asymmetry in colliding beam energies, which arises because of the usual limitation due to synchrotron radiation on e storage ring energy and which is also essential for precision measurement of scattered electrons at intermediate Q^2 ($\lesssim 100\,\mathrm{GeV}^2$), gives rise to greater instrumentation in the forward (proton beam) direction. Here a coordinate system is used with origin at the interaction point and z axis along the proton beam, or forward, direction. The pseudo–rapidity of a final state particle with polar angle θ in the laboratory is then $\eta = -\ln\tan\frac{\theta}{2}$. The very different r.f. structures of the proton and electron rings also pose the severe challenge to the experiment of e and p bunch crossings every 96 ns, a precursor for LHC experimentation. The solution is to implement "pipeline" technology in the data–acquisition stream.

Precision measurements of energy flow, charged particle production, and lepton (electron and muon) production is possible with H1 throughout a large range in laboratory pseudo–rapidity $-2.94 \leq \eta \leq 3.65$. This is achieved by means of a large asymmetric liquid argon calorimeter (LAr) with longitudinal segmentation appropriate for precision measurement of both electromagnetic ($\sigma_E/E \sim 12\%/\sqrt{E(\mathrm{GeV})} \oplus 1\%$, $\Delta E_{scale} \sim 2\%$) and hadronic ($\sigma_E/E \sim 50\%/\sqrt{E(\mathrm{GeV})} \oplus 2\%$, $\Delta E_{scale} \sim 5\%$) energy [2, 3]. ΔE_{scale} is the uncertainty in absolute value of the calorimeter energy scale. Inside the LAr is a comprehensive system of drift chambers and multi–wire proportional chambers for track measurement and triggering using charged particles originating from the z range of the event vertex (CTD, FTD). Outside the LAr is a large superconducting solenoid ($B = 1.18$ T) with an instrumented iron return yoke (CMD) plus in the forward direction a system of drift chambers and additional toroidal magnetic field (FMD) [4]. In the backward direction, scattered electrons (and positrons) are measured in the backward electromagnetic calorimeter (BEMC, electromagnetic energy resolution $\sigma_E/E \sim 10\%/\sqrt{E\,(\mathrm{GeV})}$, $\Delta E_{scale} \sim 1.5\%$) and in a multi–wire proportional chamber (BPC).

Two electromagnetic calorimeters (LUMI) situated downstream in the electron beam direction measure electrons and photons from the process $ep \to ep\gamma$ for the purpose of luminosity determination. They are also used to help quantify photoproduction background in deep–inelastic electron scattering.

In the forward direction $\eta > 3.65$, it is possible, using the "plug" calorimeter (PLUG), to "tag" the production of energy in the forward pseudo–rapidity range $3.54 < \eta < 5.08$ above a threshold of 1 GeV. Furthermore, using a novel technique [5] it is also possible to "tag" the production of hadrons in the forward pseudo–rapidity range $5.0 < \eta < 6.6$ by detecting and reconstructing

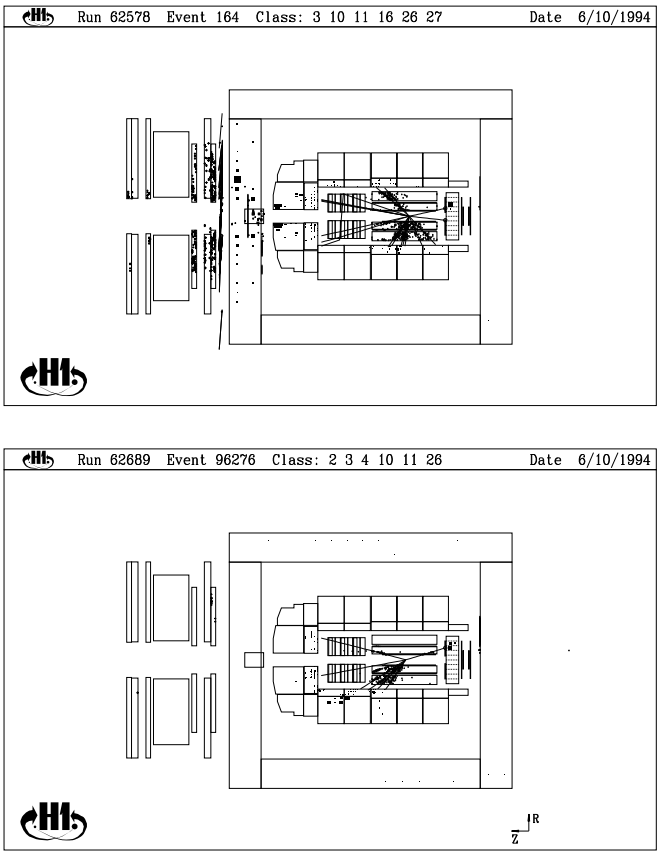

Figure 1. Two ep deep–inelastic scattering events measured in the H1 experiment at HERA. Electrons of energy 27.6 GeV are incident from the left and protons of energy 820 GeV from the right. Around the interaction point are the central and forward track detectors (CTD, FTD), the liquid argon calorimeter (LAr), the high field superconducting solenoid, and the muon detector (CMD). The upper event has hadronic fragments produced throughout the available phase space between the current direction and the forward (proton beam) direction. They are visible in the forward PLUG calorimeter and as secondaries in the foward muon detector (FMD). The lower event is an ep deep–inelastic scattering event with a rapidity gap devoid of hadronic fragments adjacent to the proton beam direction in the forward region of LAr, PLUG and FMD.

track segments in the forward muon detector (FMD) due to charged particles produced in secondary interactions of these hadrons in the collimators, the beam pipe, and adjunct material.

In 1994, the year in which much of the data were taken on which new results presented here are based, HERA delivered $6\,\mathrm{pb}^{-1}$ of integrated luminosity of which H1 used $3.9\,\mathrm{pb}^{-1}$ for physics analysis. These data consist of roughly 12×10^6 events on tape, which were recorded using triggers based on missing transverse energy in the LAr ($E_{T_{miss}} \gtrsim 6\,\mathrm{GeV}$), on track transverse momentum in CTD and FTD ($p_T \gtrsim 0.15\,\mathrm{GeV}$), on e energy in BEMC and BPC ($E_{BEMC} \gtrsim 4\,\mathrm{GeV}$ plus charged particle), and on e energy E_{LUMI} in LUMI ($0.3 < y(= 1 - E_{LUMI}/E_{beam}) < 0.7$). The integrated luminosity was measured with an accuracy of 1.5% (2%) for positron (electron) beam running. During positron beam running ($\sim 3.5\,\mathrm{pb}^{-1}$), the average $e(p)$ beam currents were 41(17) mA, and there were 168(170) $e(p)$ bunches in each ring of which 156 collided. The remaining bunches were not in collision at the interaction point and so could be used for determination of beam–gas and beam–wall/collimator backgrounds.

The configuration of the detectors which comprise H1 thus facilitates accurate reconstruction of the kinematic quantities specifying ep interactions of different nature. Furthermore, and in contrast with all its fixed target predecessors, for the first time subtle and powerful measurements of the topological features of hadron production are possible by virtue of the excellent experimental coverage of the final state phase space.

2. Kinematics

The kinematics of deep–inelastic ep physics at HERA is conveniently classified into low Q^2 and high Q^2 processes. The former correspond to quasi–real photoproduction (γp) and the latter to electroproduction. Photoproduction is in the main taken to be events for which the quasi–real photon is defined by detection and measurement in LUMI of the incident electron or positron which scatters at very small angle, and for which the factorisable approximations in for example the equivalent photon approximation and the Weizsäcker-Williams formalism can be used [6].

Deep–inelastic γp physics, like deep–inelastic (that is high p_T) proton–proton physics, requires a high p_T^2 momentum transfer squared scale (figure 2). When this is achieved in the form of production of two high p_T^2 jets, then one may write the following

$$x_\gamma \cdot x_p = \frac{M^2}{s} \qquad\qquad \frac{x_\gamma}{x_p} = \frac{t_2}{t_1}$$

in terms of the Lorentz invariant variables M^2, the CM energy squared of the parton sub–process, t_1 and t_2, the invariant 4–momentum transfers squared from the γ and p respectively to each final state parton, and s, the ep CM energy squared. The kinematic variables x_γ and x_p are well estimated from the data using the jet energies $E_T^{J_n}$ $n = 1, 2$ transverse to the γp (and ep) collision axis, and the jet pseudo–rapidities η^{J_n} $n = 1, 2$ with respect to this axis in the relations

$$x_\gamma = \frac{E_T^{J_1} \exp(-\eta^{J_1}) + E_T^{J_2} \exp(-\eta^{J_2})}{2E_\gamma} \approx x_{i/\gamma},$$

$$x_p = \frac{E_T^{J_1} \exp(\eta^{J_1}) + E_T^{J_2} \exp(\eta^{J_2})}{2E_p} \approx x_{i/p}.$$

Here $E_\gamma = yE$ is the incident (quasi–real) photon energy determined from the incident electron energy E, and

the γp centre–of–mass (CM) energy W is related to the ep collision energy $\sqrt{s}$ by $W^2 = ys$. Both x_γ and x_p may be interpreted as the fractions of the 4–momenta of the incident photon $x_{i/\gamma}$ and proton $x_{i/p}$ carried by the struck parton $i = q$ (quark) or $i = g$ (gluon) in each (figure 2b). In this way a measurement of the photoproduction of di–jets in very low Q^2 ep interactions can be used to probe the structure of the photon if the partonic structure of the proton is known, and vice–versa.

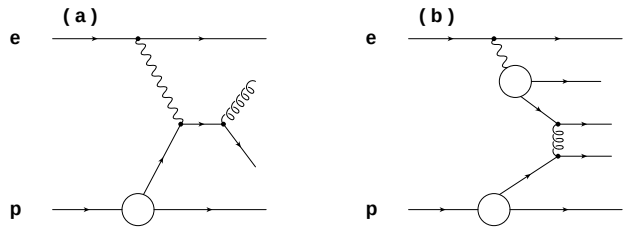

Figure 2. Schematic Feynman diagrams for a) direct γp and b) resolved γp hadron production in which jet production is observed and perturbative parton dynamics in QCD is meaningful; direct processes are sensitive only to proton structure; resolved processes are sensitive to both proton and photon structure.

High Q^2 deep–inelastic ep physics is of course best described in terms of the familiar "scaling variables" Bjorken–x x_{Bj} and Q^2 (M_p is the proton rest mass)

$$x_{Bj} = \frac{-q^2}{2P \cdot q} = \frac{Q^2}{Q^2 + W^2 - M_p^2} \approx x_{i/p} \qquad Q^2 = -q^2,$$

the former of which may be taken as the fraction of the 4–momentum of the incident proton $x_{i/p}$ carried by the "struck" parton, that is the parton coupling to the virtual photon (figure 3). Here q and P are the 4–momenta of the virtual boson and the incident proton respectively.

However at HERA the immense ep CM energy ($\sqrt{s}$), and the access to the final state hadronic phase space in the form of the large coverage in pseudo–rapidity η afforded by the colliding beam laboratory frame, mean that this well known picture can be extended. Suppose that a proportion, M_X, of the total hadronic invariant mass W (W equals the $\gamma^* p$ CM energy) can be defined in an interval of η adjacent to the direction of the current quark (figure 3). Then, the fraction of the 4–momentum of the incident proton carried by the system S, which together with the virtual photon constitutes X, can be written

$$\begin{aligned} x_S &= \frac{q \cdot (P - P')}{q \cdot P} \\ &= \frac{Q^2 + M_X^2 - t}{Q^2 + W^2 - M_p^2} \\ &\approx \frac{Q^2 + M_X^2}{Q^2} \cdot x = x_{S/p}, \end{aligned} \qquad (1)$$

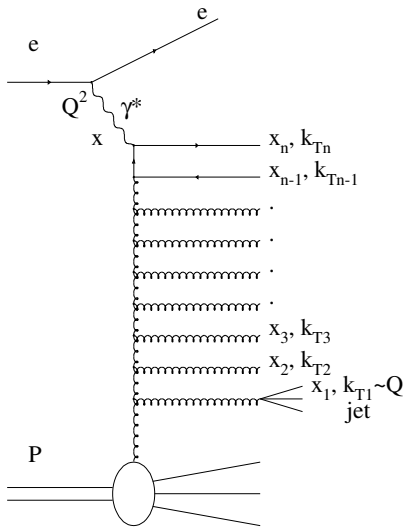

Figure 3. Schematic Feynman diagram for ep DIS at low Bjorken–x illustrating how QCD can give rise to hadron production from partons produced between the "struck" or "current" quark and the proton remnant; increasing pseudo–rapidity η from the current quark towards the remnant corresponds roughly to increasing the fractional momentum $x_{i/p} = x_i$ of the parton which forms the side of the "ladder"(usually a gluon at low Bjorken–x) as a fraction of the incident proton; the transverse momenta of the ith parton is k_{Ti}.

Also the fraction of the 4–momentum of S carried by the quark coupling to the virtual photon can be written

$$\begin{aligned} \beta &= \frac{-q^2}{2q \cdot (P - P')} = \frac{Q^2}{Q^2 + M_X^2 - t} \\ &\approx \frac{Q^2}{Q^2 + M_X^2} = x_{q/S}. \end{aligned} \qquad (2)$$

Here the 4–vector of S is specified by $P - P'$ and its space–like mass squared by $t = (P - P')^2$. Note as expected that

$$x = \beta \cdot x_S, \qquad (3)$$

and that the compact interpretation of x, x_S and β as fractional momenta are only valid in the low "mass" limits $\mid t \mid$, $M_p^2 \ll Q^2, M_X^2$. In the cases normally considered, namely when S is a gluon from the proton (see section 6 below) or S is a colourless momentum transfer coupling to the proton (see section 8 below), t easily meets such a requirement. The simple multiplicative relationship in equation 3 between fractional momenta x, β and x_S is a specific case of the fact that moving in pseudo–rapidity η from the current towards the proton remnant corresponds to fractional momenta x increasing from x_{Bj} such that $\Delta \ln x = \Delta \eta$.

3. Impostors at a Deep–Inelastic Workshop

Though strictly speaking not of relevance to a DIS workshop, new measurements of the total photopro-

duction cross section $\sigma^{\gamma p \to X}$ and the total cross section $\sigma^{\gamma p \to \rho p}$ for $\rho(770)$ photoproduction have recently been made by H1. Both are important measurements in their own right, and both are also examples of processes which must be understood at least phenomenologically at HERA energies if measurements amenable to perturbative QCD, such as deep–inelastic processes, are to be made reliably. The results are:

$$\sigma^{\gamma p \to X}_{W=197\,\mathrm{GeV}} = 165.3 \pm 2.3(\mathrm{stat.}) \pm 10.9(\mathrm{syst.})\,\mu\mathrm{b}\ [7]$$

$$\sigma^{\gamma p \to \rho p}_{W=55\,\mathrm{GeV}} = 11.4 \pm 0.8(\mathrm{stat.}) \pm 2.5(\mathrm{syst.}) \pm 0.6(\mathrm{lumi.})\,\mu\mathrm{b}. \quad [\mathrm{preliminary}]$$

Both measurements are in excellent agreement with theoretical expectation based on low energy Regge phenomenology applied to a hadronised (vector meson dominated – VMD) photon. This is specified by a leading effective trajectory (the pomeron $I\!P$) of the form consistent with all hadronic diffraction [8, 9].

4. Deep–Inelastic $p\gamma$ Physics

Quasi–real hadronic photoproduction events can be selected in H1 by requiring a LUMI "tag" together with at least one track in the CTD as trigger. Off–line analysis of course yields only a proportion of these events as deep–inelastic candidates by virtue of the requirement of two or more jets, each with transverse energy $E_T \geq 7\,\mathrm{GeV}$ (transverse to the common ep and γp beam axes). In addition cuts are applied to ensure both that the jets are fully contained in the LAr ($0 \leq \eta^{J_n} \leq 2.5$ $n = 1, 2$), and that there is no possibility at small angle of an energetic remnant from the photon being included as a high E_T jet ($\Delta\eta^{J_n} \leq 1.2$). Jets are defined with a cone algorithm following the Snowmass accord, namely with $R = \sqrt{(\Delta\eta)^2 + (\Delta\phi)^2} = 1$ (η and ϕ are here pseudo–rapidity and azimuth respectively and they are specified relative to the $ep/\gamma p$ beam axis).

The resulting jet cross sections can then be measured and compared with QCD expectation [10, 11]. The latter depends on both the parton sub–processes involved and the parton densities in the photon and the proton, as well as the complication of parton hadronisation. Models, which are more or less reliable, exist for the latter. The sub–processes of relevance depend on the order of truncation of the QCD perturbative expansion. The distinction between what is partonic hadronisation and what are the perturbative partonic sub–processes remains at some level obscure. Nevertheless, in leading order (LO) in QCD in which the parton diagrams are well known and calculable, it has been found possible to unfold from the jet cross sections to the parton cross sections (figure 4 in which the theoretical curves are from [11, 12, 13]). Additional systematic errors of course arise due to our ignorance of the precise nature of hadronisation. Finally, because the range of x_p is restricted kinematically to $x_p \gtrsim 0.01$ for which the parton distribution functions (pdfs) of the proton are relatively well known from measurements of ep DIS, the LO parton content of the photon can be extracted.

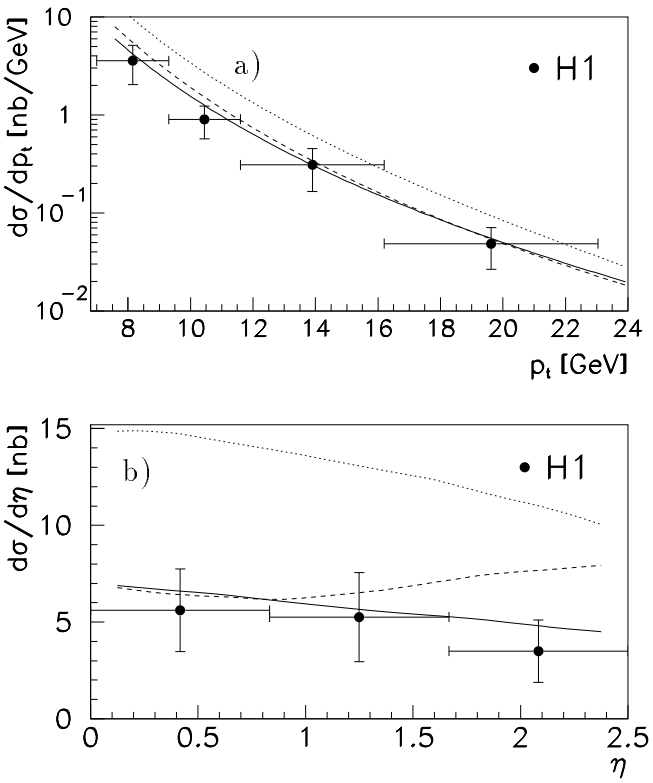

Figure 4. Parton differential cross sections a) $\mathrm{d}\sigma/\mathrm{d}p_T$ and b) $\mathrm{d}\sigma/\mathrm{d}\eta$; the continuous (discontinuous) curve is the prediction from the Kramer–Salesch (Abramowicz et al.) QCD calculation.

For the results shown, the GRV [14] pdfs, evaluated assuming LO Dokshitzer, Gribov, Lipatov, Altarelli, Parisi (DGLAP) QCD evolution [15], are used for the proton (with a systematic uncertainty of ±15%). The distribution of deep–inelastic $p\gamma$ interactions as a function of x_γ (figure 5a) reveals a contribution at $x_\gamma \sim 1$ corresponding to the direct coupling of the incident photon (with no intrinsic spatial extent - see figure 2a) with a quark which may be attributed to proton structure. The contribution for $x_\gamma < 1$ is thus taken to be due to resolved photon interactions (see figure 2b) in which the hard scattering is attributed to partons from both proton and photon structure. Because the quark component of the latter is known to useful precision from deep–inelastic $e\gamma$ measurements of the photon structure function F_2^γ at e^+e^- colliders [16, 12, 13], it is then possible to extract evidence for gluon sub–structure in the photon. The contribution of the quark component, calculated from e^+e^- measurements,

is shown in figure 5a). There is a clear excess at low x_γ – the probability that quarks alone make up photon sub–structure which contributes to resolved photoproduction (in LO) is found to amount to less than 0.1%. It is even possible to extract a LO gluon pdf for the photon at a scale $p_T^2 = 75\,\mathrm{GeV}^2$ (figure 5b). Though the overall errors are large, one can already see that the solutions which are admissable using e^+e^- measurements only [12, 13] and which involve large contributions at low x_γ are unlikely.

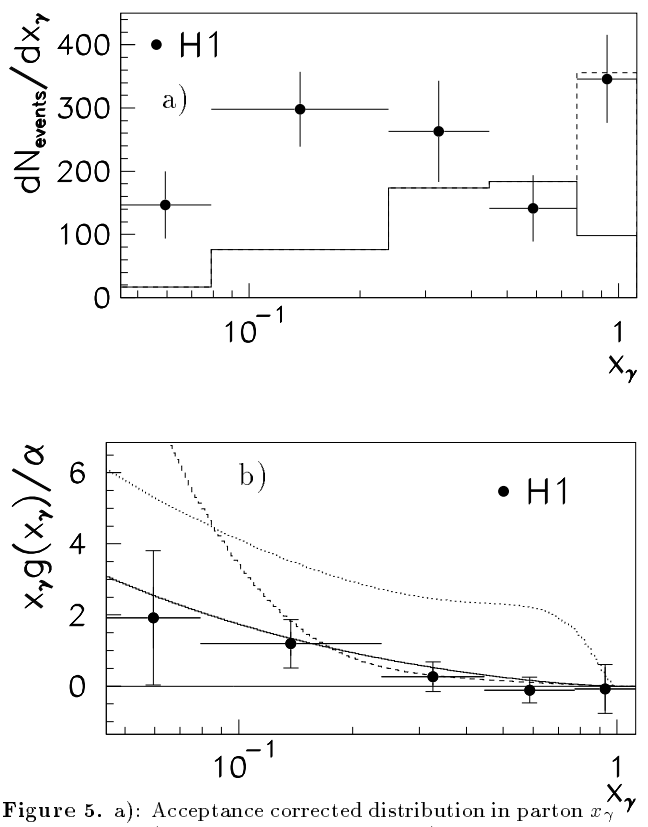

Figure 5. a): Acceptance corrected distribution in parton x_γ showing direct ($x_\gamma \to 1$ - dashed histogram) and resolved ($x_\gamma < 1$ - continuous histogram) γp interactions; b): gluon distribution function $x_\gamma g(x_\gamma)$ in the real photon; the continuous (discontinuous) curve is from the GRV (Abramowicz et al.) QCD analysis, both of $e\gamma$ DIS data.

For the first time a first glimpse of the gluonic contribution to the hadronic structure of the photon is possible. Following years of persistent and difficult measurement at e^+e^- colliders in which the sensitivity to gluon photon structure has been through QCD evolution only, this is an important step at getting directly at the gluon component. The hadronic structure of the photon is a uniquely important measurement of the way QCD vacuum fluctuations build an effective spatial extent for an otherwise point–like gauge boson, and resolved photoproduction is now the best way of measuring the gluonic pieces.

5. Deep–Inelastic *ep* Physics: the Proton Structure Function F_2

5.1. Low x_{Bj} Proton Structure

The progenitor of deep–inelastic ep physics is the measurement of the deep–inelastic ep structure functions, F_1 (or F_L) and F_2, in the inclusive process $ep \to eX$ at high Q^2. In terms of the variables Bjorken–x, Q^2, and $y = \frac{Q^2}{sx}$ (see above), the cross section $\frac{\mathrm{d}^2\sigma_{ep\to eX}}{\mathrm{d}x_{Bj}\mathrm{d}Q^2}$ can be written:

$$\frac{\mathrm{d}^2\sigma_{ep\to eX}}{\mathrm{d}x_{Bj}\,\mathrm{d}Q^2} = \frac{4\pi\alpha^2}{Q^4 x_{Bj}}\cdot[1-y+\frac{1}{2}\frac{y^2}{1+R}]\cdot F_2(x_{Bj},Q^2) \quad (4)$$

where α is the fine structure constant and where account is taken only of the electromagnetic piece of the electroweak coupling of the incident e. The quantity $R = \frac{F_2}{2x_{Bj}F_1} - 1$ is the ratio of the virtual photon–proton longitudinal to transverse cross sections ($R = \sigma^{\gamma_L^* p\to X}/\sigma^{\gamma_T^* p\to X}$). There is relatively little sensitivity to R in equation 4 because the data are mainly at small y by virtue of the e QED vertex and virtual photon exchange. In the results presented here the QCD expectation for R is assumed [17]. In the last 25 years, measurements of F_2 have formed the basis of our interpretation of proton structure in terms of valence quarks (flavour non–singlet), and sea quarks plus gluons (flavour singlet).

Precise measurements of F_2, together with the machinery of perturbative QCD in the form of DGLAP evolution, have yielded solutions for the non–singlet and singlet quark and gluon pdfs for $x_{Bj} \gtrsim 0.01$. To get to lower x_{Bj} requires higher ep CM energy $\sqrt{s}$ for a given Q^2. Since its inception, experiments at HERA have thus accessed a new kinematic region of ep DIS which has developed to the extent that we have now first measurements of pdfs for $x_{Bj} \gtrsim 10^{-3}$ using measurements of F_2 for $x_{Bj} \gtrsim 8\times10^{-5}$ and $Q^2 \geq 3.5\,\mathrm{GeV}^2$.

This extension in kinematic range is into hitherto unexplored territory. Intuitively in QCD one expects a large and increasing gluon contribution to proton structure as x_{Bj} decreases, and this is born out in practice by the DGLAP truncation of the perturbative expansion becoming questionable by virtue of leading $\ln\frac{1}{x}$ terms which arise inevitably in gluon Bremsstrahlung. An approach which attempts to address this kinematic region in x_{Bj} more appropriately is due to Balitskiĭ, Fadin, Kuraev and Lipatov (BFKL) [18], but it does so in a way which does not encompass the established DGLAP approach at higher x_{Bj}. New "low x measurements" at HERA of F_2 thus pose the challenge not just of extracting the partonic structure of the proton at low x where flavour singlet domination is expected, but also of specifying the development of QCD perturbative technology

which is necessary to understand dense partonic systems. With this challenge comes the excitement of the possibility of discovering new phases of partonic matter, for example "hot spots" [19, 20], and, with the powerful lever arm in Q^2, of observing their evolution to real (soft, non–perturbative) $Q^2 = 0$ photon processes.

5.2. Experimental Technique

The data used to evaluate F_2 in equation 4 above are taken by requiring a scattered electron (positron) with sufficient energy $E' \gtrsim 5\,\mathrm{GeV}$ to trigger in the BEMC and BPC (typical events are shown in 1). Off–line the kinematics are reconstructed using both the scattered e and the hadronic final state [21, 22]. There is redundancy in determining Q^2 from e, and then y from either or both of the scattered e and the hadronic quantity $E_{had} - P_{z\,had}$ which is well measured in the LAr (E_{had} is the total hadronic energy measured and $P_{z\,had}$ its z component) [23]. This facilitates powerful cross checks at many stages of the analysis, in particular concerned with the effects of radiative corrections and with the lack of any good y measurement from the scattered e at low y. The final data sample is selected to be within well understood "fiducial ranges" in Q^2 measured in the BEMC and the LAr. The use of hadrons for y measurement means that measurements of F_2 can be made for $y \leq 0.01$, and thus to extend in x_{Bj} to reach lower energy fixed target experiments. The necessary accuracy is achieved by a judicious combination of track measurement in the CTD and energy cluster measurement in the LAr. The final data sample requires $E' \geq 8\,\mathrm{GeV}$. The small level of background from photoproduction processes which can fake a good e tag and survive the kinematic analysis above is quantified by Monte Carlo simulation and comparison with DIS ep candidates which also have energy tagged in LUMI.

The most significant experimental development since first results for F_2 were presented and the large rise of F_2 was discovered in 1993 [24, 25] has been measurements of the x_{Bj} dependence of F_2 at lower Q^2. The kinematic range is extended by moving the HERA ep interaction point forward by about $\Delta z = +67\,\mathrm{cm}$ so that the lower limit in e scattering angle which can be measured in the BEMC is "reduced" (remembering the H1 co-ordinate frame) from 173^o to 175.5^o (figure 6). Also, more by luck than judgement, the difficult r.f. structure in HERA gives rise in the interaction region to a second "satellite bunch" of protons about $\Delta z = +70\,\mathrm{cm}$ from the nominal interaction point. There is enough integrated luminosity in this satellite bunch to give an on–going cross check of the shifted vertex analysis for lower Q^2 measurements throughout data taking. Following a successful "proof of method" measurement by H1 in 1993 in which first measurements were obtained [21], new more accurate preliminary results are presented here for the first time at $Q^2 = 3.5\,\mathrm{GeV}^2$, and it will be possible in the final analysis to obtain results down to $Q^2 = 1.5$ to $2\,\mathrm{GeV}^2$.

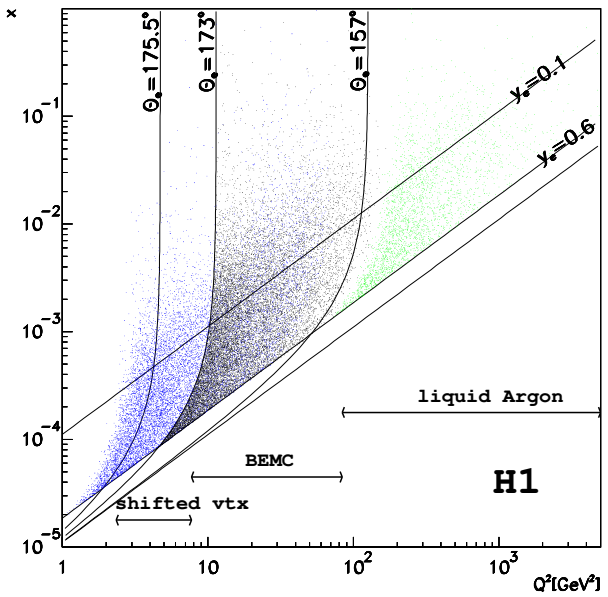

Figure 6. Selected ep DIS events in H1 1994 data showing the extension to low x_{Bj} of shifted vertex data taking.

5.3. Results for $F_2(x_{Bj}, Q^2)$

Results presented here (April 1995) correspond to a snapshot of the on-going H1 analysis for F_2. It includes recently published results from data taken in 1993 [21] as well as preliminary results from 1994 data taking. Figure 7 summarises the 1993 measurements in the form of the x_{Bj} dependence at fixed Q^2 and vice–versa. In the former the effect of the low y reach is clearly visible in the first confrontation, after little or no extrapolation, of fixed target and HERA collider data, revealing impressive agreement. There is indisputable evidence for substantial scaling violations in the form of a rising Q^2 dependence of F_2 – the classic signal of a major contribution from gluons to hadronic structure – in the region of low x_{Bj} which exhibits the rising x_{Bj} dependence as x_{Bj} decreases. Moreover the results are consistent with, but do not yet require, this Q^2 dependence to become steeper as x_{Bj} decreases. Such a trend is expected if the rise of F_2 with decreasing x_{Bj} at sizeable Q^2 is to be consistent with the W dependence of $\sigma^{\gamma p \to X}$.

Superimposed on the x_{Bj} dependences at fixed Q^2 is a best fit to a QCD next–to–leading order (NLO) DGLAP fit in which the minimum possible ansätze are made for the gluon, quark flavour singlet, and

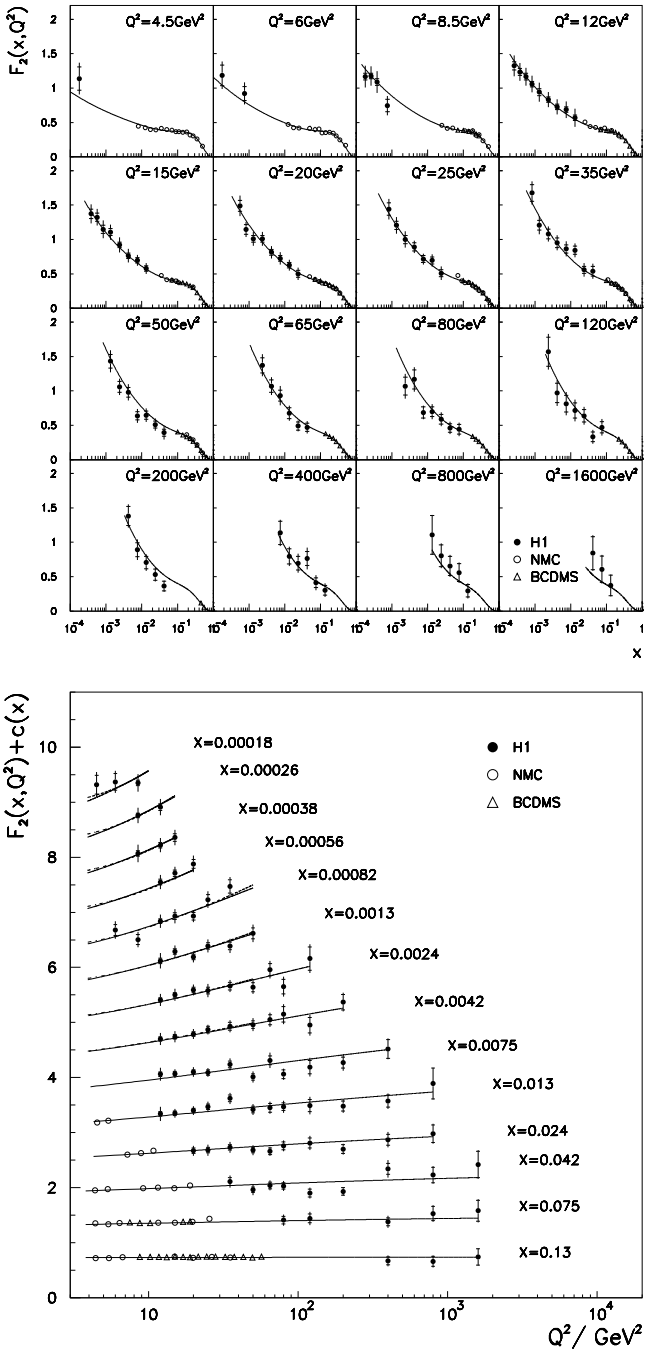

Figure 7. The proton structure function F_2 as a function of Bjorken–x at fixed Q^2 (top) and as a function of Q^2 at fixed Bjorken–x (bottom; note the scaling factor for display purposes $c(x) = 0.6(i_x - 0.4)$ where i_x increments from 1 at $x_{Bj} = 0.13$); superimposed on the x_{Bj} dependence is the result of a NLO DGLAP QCD fit; superimposed on the Q^2 dependence are the results of a LO order DGLAP QCD fit (continuous curve) and a mixed LO DGLAP/BFKL QCD fit (dashed curve).

quark flavour non–singlet distributions, and in which the usual momentum sum rule is assumed [26]. Also included are data sets from fixed target measurements by NMC [27] and BCDMS [28] for which $Q^2 < 4\,\mathrm{GeV}^2$ for $x_{Bj} < 0.5$ (kinematics) and $Q^2 > 15\,\mathrm{GeV}^2$ for $x_{Bj} > 0.5$ (to avoid higher twist QCD diagrams). There is remarkable agreement with measurements over a huge kinematic domain $0.00018 \leq x_{Bj} \leq 0.13$ and $4.5 \leq Q^2 \leq 1600\,\mathrm{GeV}^2$ ($\Lambda_{\overline{MS}} = 215\,\mathrm{MeV}$, evolution starting scale $Q_0^2 > 4\,\mathrm{GeV}^2$). This agreement is an impressive monument to our understanding of proton structure in terms of QCD.

The 1994 data analysis is still in progress. However preliminary results are already available (figure 8) for some of the lower Q^2 ($\leq 25\,\mathrm{GeV}^2$) region which includes $60\,\mathrm{nb}^{-1}$ of shifted vertex data. The rise of F_2 with decreasing x_{Bj} is now clearly visible in the H1 data alone for $Q^2 \lesssim 5\,\mathrm{GeV}^2$.

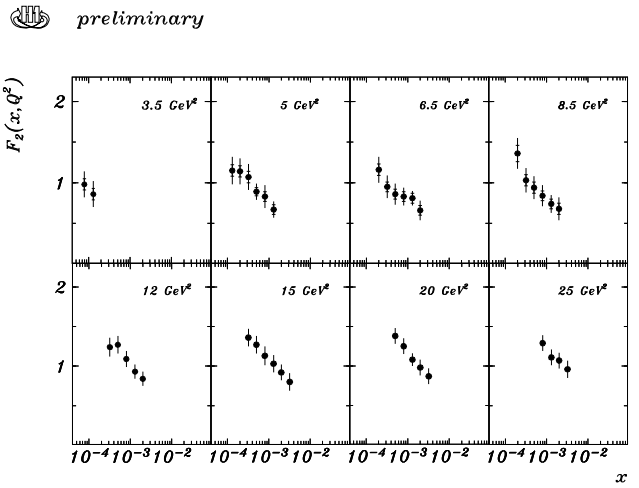

Figure 8. The proton structure function F_2 as a function of Bjorken–x at low Q^2 determined using data taken in 1994 in which the ep interaction vertex was shifted to provide measurements at lower Q^2; the rise with decreasing x_{Bj} of F_2 is confirmed down to $Q^2 = 3.5\,\mathrm{GeV}^2$.

5.4. The Gluon Content of the Proton

Of particular interest from the NLO QCD analysis is the gluon pdf. It is shown as a function of x (here $x = x_{g/p}$ in the kinematic terms of section 2 above) in figure 9, where it can be seen to rise steeply with decreasing x. At $Q^2 = 20\,\mathrm{GeV}^2$ and for $x \geq 1.8 \times 10^{-4}$, the gluon density in the proton is well described by $xg(x) \sim x^{-0.23}$. The interesting question is whether the gluon density can be considered large enough for the inevitable breakdown in the QCD evolution equations. This breakdown must arise when saturation occurs, that is when non–linear effects required by unitarity occur in which coloured partons shield each other and gluons recombine. Simple estimates [20] suggest that saturation is unimportant for $xg(x) \lesssim 6Q^2(\mathrm{GeV}^2)$, that is for $\lesssim 6Q^2(\mathrm{GeV}^2)$ gluons per unit rapidity interval. Present measurements therefore

indicate that for $x \geq 1.8 \times 10^{-4}$ "there is room in the proton for more gluons".

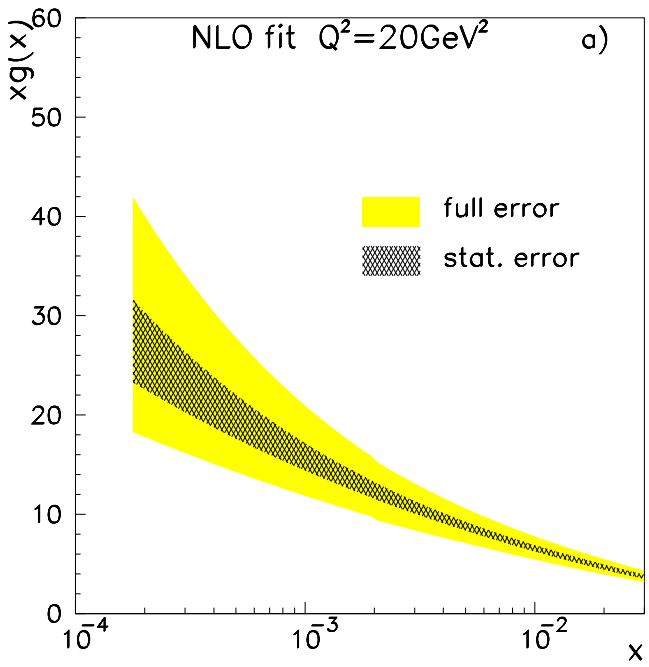

Figure 9. The gluon distribution function in the proton $x_{g/p}g(x_{g/p})$ at $Q^2 = 20\,\mathrm{GeV}^2$ extracted from a NLO DGLAP QCD fit of the Q^2 evolution of the proton structure function F_2.

5.5. Search for New QCD Effects

An interesting question in low x_{Bj} proton structure concerns the possibility of BFKL QCD dynamics. This has been investigated in LO using a mixed BFKL and DGLAP parametrisation of the (x_{Bj}, Q^2) domain of F_2. Below $x = x_0$ DGLAP evolution of $xg(x)$ (in Q^2 assuming a parametrisation in x at starting scale $Q_0^2 = 4\,\mathrm{GeV}^2$) is replaced by BFKL evolution (in x requiring continuity of $xg(x)\frac{\mathrm{d}[xg(x)]}{\mathrm{d}\ln Q^2}$ at $x = x_0$). A fit to the 1993 H1 results ($Q^2 \leq 50\,\mathrm{GeV}^2$), together with fixed target measurements by NMC and BCDMS, reproduces the measurements well with $x_0 \sim 4 \times 10^{-3}$ and is almost indistinguishable from a LO DGLAP fit (figure 7). The precision of the 1993 measurements is therefore inadequate to distinguish BFKL dynamics in the context of such a fit.

5.6. Conclusion

It is clear that our understanding of proton structure at low x_{Bj} is at a watershed following a triumphant beginning in which measurements in H1 have established the rising behaviour with decreasing x_{Bj} of F_2 and its culmination in a determination of the gluon density in the proton. The experimental precision is now dominated by systematic uncertainties, and at the present level of accuracy one is barely able to resolve the simplest modelling of new QCD dynamics. The future is one of "hard grind" to reduce systematic errors and one of imaginitive new experimental measurement, for example of F_L and of F_2 at even lower Q^2. The rewards in terms of new insight into QCD demand that this effort continue to its limits.

What is not yet limited in any way by systematic effects is measurement of the proton structure functions at the highest possible Q^2. This more conventional region of proton structure at higher x_{Bj} can be probed with a 10–fold increase in spatial precision using both neutral current and charged current electroweak interactions. Such measurements are the stuff of quark structure, in the form either of anomalous QCD effects or of a new level of the sub–structure of matter, and they will only be possible when HERA is able to deliver significantly higher luminosity than to date.

6. Deep–Inelastic *ep* Physics: Jets and Partons in Low x Physics

6.1. Introduction

An understanding of proton structure in QCD requires not just consistency with the totally inclusive cross section measurements in the form of proton structure functions, but also an understanding of the hadronic final state. The excellent coverage of H1 at HERA combined with the wide open access to hadronic measurements in a collider experiment is revolutionising this aspect of ep DIS.

The safest path to tread in addressing the complexities of the hadronic final state in ep DIS is to work in a perturbative QCD domain. This is achieved by studying the production of jets, defined again using the Snowmass accord (see above) or using a clustering algorithm more acceptable to perturbative QCD treatment and interpretation [29]. To $O(\alpha_S)$ in QCD, the diagrams amount to the classic parton model plus inelastic Compton scattering and boson–gluon fusion (figure 10). The immense phase space at HERA, by virtue of the large W in low x_{Bj} DIS, means that multi–jet identification is possible with good efficiency, and, just as in the $p\gamma$ DIS measurements in section 4 above, one can anticipate unfolding to extract the $O(\alpha_S)$ parton dynamics. This has been achieved in the ep DIS sample (requiring in addition that $W^2 > 3000\,\mathrm{GeV}^2$), and the results used to draw conclusions concerning QCD dynamics and proton structure.

6.2. Determination of the QCD Coupling α_S

The diagrams in figure 10 clearly imply a sensitivity to QCD α_S of the proportion R_{2+1} of the ep DIS cross

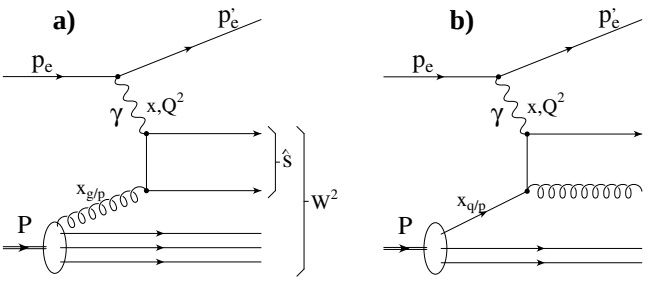

Figure 10. $O(\alpha_S)$ QCD diagrams which contribute to $2+1$–jet production in ep DIS; a) boson–gluon fusion, b) QCD Compton.

section which is $2+1$ jet. Here the cross sections σ_{2+1} and σ_{1+1} refer to the production of 2 jets and 1 jet, with a "beam–pipe" remnant from the proton (+1) remaining at low p_T with respect to the p beam axis whose existence can only be inferred kinematically. The analysis is able to unfold to a parton level and then extract a Q^2 dependence of α_S in NLO. The result is in figure 11 [30]. There is strong suggestion that α_S "runs" as it should as a function of Q^2. Moreover a value of $\alpha_S(M_Z^2) = 0.123 \pm 0.018$ is obtained, which compares well with other processes [31].

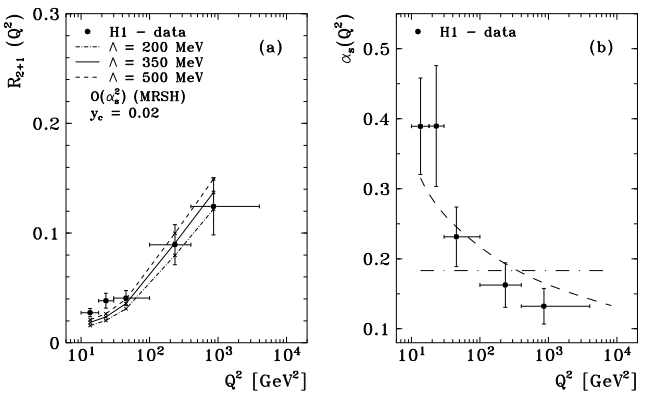

Figure 11. a) The proportion R_{2+1} of the ep DIS cross section which is $2+1$ jet as a function of Q^2; b) QCD coupling constant α_S extracted from R_{2+1} as a function of Q^2.

6.3. Direct Determination of the Gluon Density in the Proton

Because the diagrams in figure 10 are also known quantitatively if we can believe QCD (including knowledge of α_S!), then a procedure much along the lines in section 4 can be used to attempt to extract the pdfs of the proton. The results justify the method in that a measure of $xg(x)$ in LO is achieved which broadly agrees with the more traditional technique using the Q^2 evolution of the structure function F_2 (section 5) [32] and with the electroproduction of J/ψ [33]. Here x is now $x_{S/p} = x_{g/p}$ which is measured by defining the mass M_X in the kinematic equations 1 and 2 above to be the two jet mass. There are some caveats which make for contributions to systematic uncertainty much as in the case of $p\gamma$ DIS and photon structure. Nevertheless it is encouraging that the first attempt to correlate perturbative aspects of the ep DIS final state with QCD expectation can be understood in terms of the simplest LO interpretation of the gluonic content of the proton. The QCD picture seems to be as it should in its simplest expectation (figure 12).

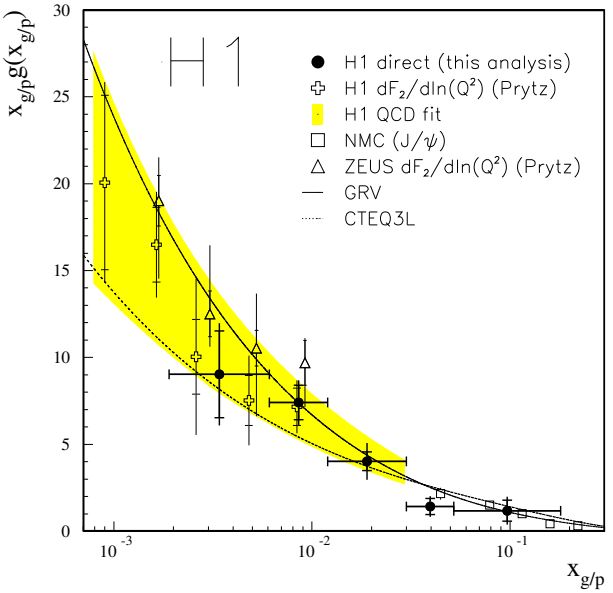

Figure 12. The gluon distribution function in the proton $x_{g/p}g(x_{g/p})$ extracted from a measurement of the rate for $2+1$ jet production; also shown are the results for $x_{g/p}g(x_{g/p})$ from different approachs in LO QCD analysis of the proton structure function F_2 and from a measurement of the electroproduction of J/ψ.

6.4. Summary

Together, both these results signal clearly that to date QCD as we believe in it (DGLAP) works well in describing the way jets are produced in low x_{Bj} ep DIS.

7. Deep–Inelastic ep Physics: Hadronic Energy Flow and Forward Jet Production

7.1. Introduction

The real challenge to QCD in hadronic physics is an understanding of hadron production in toto, for example hadronic energy flow, in inelastic collisions. DIS ep is a good testing ground because it stands some chance of being amenable to perturbative calculation due to the existence of at least one hard scale Q^2. This having been said, however, it is not hard to see that LO diagrams such as those in figure 10 have divergences which are only controllable when a second momentum scale exists in the form of a "$\hat{p}_T$ cut–off". This requirement is met

in a multi–jet analysis with significant p_T, but it is not met in full energy flow measurements.

Nevertheless there exist Monte Carlo based models of the total ep DIS final state [34, 35] which can be compared with observation. They are complicated, carry the stamp of theoretical respectability, and are a little opaque (at least to this experimentalist!) when it comes to distilling out the essential characteristics in the data which lead to a meaningful interpretation. One distinguishing feature between two of them, based on matrix element and parton showers (MEPS - LEPTO6.1) [34] and on the colour dipole model (CDM) [35], is that in the former there is an ordering of momentum transfer in the partonic ladder ($k_{tn} > k_{t(n-1)} > k_{t(n-2)} > ...$ in figure 3) which inevitably builds the hadronic final state, and in the latter there is not. The former is in fact based on DGLAP evolution, and it turns out that such momentum transfer ordering, in which k_T increases from the proton up to the virtual photon, is inevitable in such an approach. In contrast it seems to be the case that a BFKL view of parton dynamics does not require this k_T ordering. Perhaps by miraculous coincidence, perhaps not, the CDM Monte Carlo simulates partons which are not ordered in any way in momentum transfer, so that the door is open to see if the data prefer such ordering or not.

7.2. Energy Flow and BFKL

Already H1 has published a detailed study of the transverse energy flow $\frac{dE_T}{d\eta}$ as a function of laboratory pseudo-rapidity in which it is clear that straight application of MEPS undershoots the data (figure 13) away from the struck quark (or current) direction (figure 3) [36]. This work has now progressed to consider the energy flow in the $\gamma^* p$ rest frame between the current and the virtual photon.

Calculation at the parton level in BFKL QCD has been shown to produce about 40 times more transverse energy than in DGLAP QCD at low x_{Bj} and to have a dependence of average transverse energy $< E_T^* >$ on x_{Bj} which could be different from DGLAP QCD [37]. The region of pseudo–rapidity η^* in the $\gamma^* p$ rest frame away from the current–proton axis is the region in the perturbative ladder (figure 3) between the current and the proton where the sensitivity to the presence or absence of ordering is maximal in $< E_T^* >$.

Figure 14 shows $< E_T^* >$ as a function of x_{Bj} together with the CDM expectation at both the parton and the hadron level to illustrate the possible effect of hadronisation [38]. Also shown is the parton level calculation by Kwiecinski et al [37]. If indeed CDM mimics BFKL parton dynamics and subsequent hadronisation, then things look exciting. But caution is called for – there is enough freedom in MEPS simulation in for example the choice of $\hat{p}_T$ cut–offs and proton pdfs to fix things up [39, 38]. The best that can be said is that there is no experimental evidence yet to require the addition of BFKL in the entirety of DGLAP based QCD technology which describes energy flow in low x_{Bj} ep DIS. But equally, and significantly because DGLAP must ultimately fail at small but finite x_{Bj}, there is no experimental reason yet to reject it.

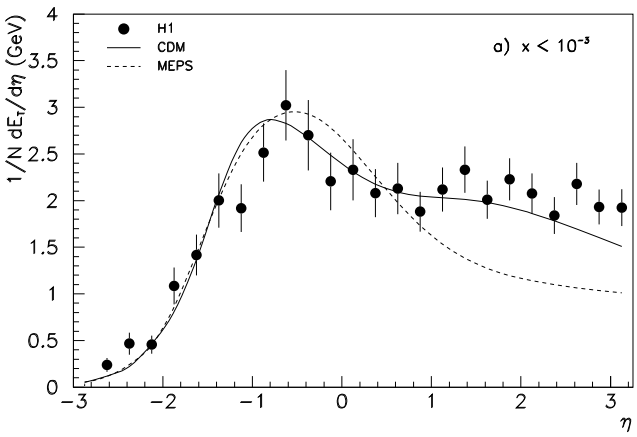

Figure 13. Average laboratory transverse energy $< E_T >$ as a function of laboratory pseudo–rapidity in low x_{Bj} ep DIS compared with Monte Carlo simulations MEPS and CDM (see text).

7.3. Forward Jet Production and BFKL

A tantalising exercise which abandons straight total energy flow by returning again to a guaranteed perturbative approach and jet production, and which may turn out to be more definitive as regards BFKL, follows a suggestion by Mueller et al. [20, 40, 41] to look carefully at forward jet production in ep DIS at low x_{Bj}. The idea is beautifully simple – the energetic jet is at sufficient $x_{jet/p}$ and p_T^2 with respect to the proton to ensure that there is a second hard scale in addition to Q^2 in the partonic ladder (figure 3) with a large interval in x between it and the struck quark at $x_{q/p} = x_{Bj}$. Such a large kinematic bite in x at low Bjorken–x is sensitive to perturbative BFKL evolution. The latter predicts a very different jet production cross section than perturbative DGLAP.

The results are to date preliminary, and are based on the following cuts: $x_{jet/p} > 0.025$, $0.5 < \frac{p_T^2}{Q^2} < 4\,\mathrm{GeV}^2$, $6 < Q^2 < 20\,\mathrm{GeV}^2$ and $p_T > 5\,\mathrm{GeV}$. They are presented in table 1 both as a comparison of observed number of such jets in H1 with expectation based on the CDM and MEPS simulations, and as cross sections [42, 38]. CDM wins, confirming that a Monte Carlo with no explicit parton ordering is favoured.

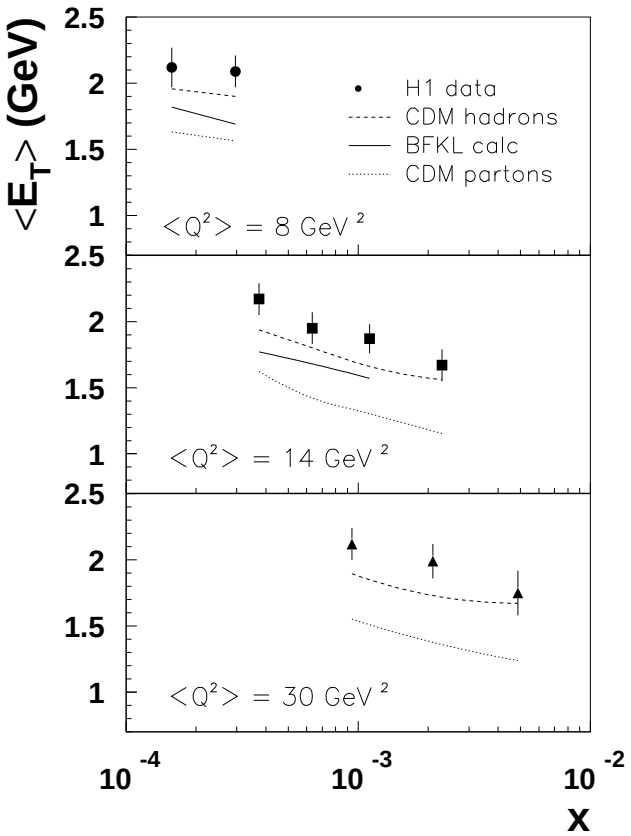

Figure 14. Average laboratory transverse energy $< E_T >$ as a function of Bjorken–x compared with the CDM simulation excluding and including hadronisation and with a parton level calculation (see text), demonstrating the suggestion that there may be evidence for better agreement with dynamics which does not include ordering in parton transverse momenta, as in the BFKL QCD approach.

Bjorken x ($\times 10^{-3}$)	events obs.	MEPS	CDM	σ (pb) $\pm$ stat. $\pm$ syst.
0.2 to 1.0	304	136	271	$760 \pm 45 \pm 155$
1.0 to 2.0	162	97	104	$469 \pm 39 \pm 88$

Table 1. Uncorrected rates for events (obs.) with a forward high p_T jet in two different regions of Bjorken–x in low x_{Bj} DIS compared with the expectations from two simulations, MEPS and CDM (see text); also shown are the cross sections; the measurements are made assuming cuts as specified in the text.

7.4. Energy Flow and High Energy Hadron Physics

Many years ago, Bjorken and Kogut proposed that the structure of the DIS final state would follow the general features of all hadronic physics [43]. In essence the hadronic final state should be distributed in rapidity between the beam particles (the virtual photon and the proton) in a manner in which the dynamics could be associated with each at each end of the distribution, and otherwise would be independent of them in the central region. This is indeed found to be the case in all high energy hadron–hadron interactions. Whether γp and $\gamma^* p$ fit into such a picture is an interesting and important question in view of our pictures of photoproduction and DIS in terms of photon hadronisation or otherwise.

By studying the dependence of transverse energy density $\frac{1}{\eta^*}\frac{\mathrm{d}E_T}{\mathrm{d}\eta^*}$ (for $0.3 \leq y \leq 0.7$) on η^*, the pseudo-rapidity in the $\gamma^* p$ CM system, a comparison with the Bjorken/Kogut picture has been made (figure 15a) [44]. Any growth of E_T^* with $0 \leq Q^2 \leq 520\,\mathrm{GeV}^2$ is seen only to be significant in the current region (where a perturbative QCD treatment of a virtual photon naturally predicts it). Towards the central region there is little or no sensitivity of $\frac{1}{\eta^*}\frac{\mathrm{d}E_T}{\mathrm{d}\eta^*}$ to Q^2, that is to the mass of the photon, exactly as the Bjorken/Kogut picture predicts. Furthermore in the region as close to the central region as measurements permit ($\eta* = 0$), $[\frac{1}{\eta^*}\frac{\mathrm{d}E_T}{\mathrm{d}\eta^*}]_{\eta*=0}$ has no significant dependence on Q^2, and moreover shows no significant difference from soft pp physics at the same CM energy W (figure 15b) [45]. The central rapidity region in DIS seems to be identical to that in soft hadronic physics, and the Bjorken/Kogut picture seems to be valid.

7.5. Conclusion

There are thus tempting hints in the ep DIS hadronic final state of the extensions necessary to DGLAP QCD dynamics at low x_{Bj}. Whether they survive the tests of future careful scrutiny is unclear. The excitement concerning the possibility that these extensions may be as proposed by BFKL is based partly on measurements of energy density in the central region of the $\gamma^* p$ rapidity distribution. Because of the similarity of this energy density with pp interactions, if a signature of BFKL dynamics can be established in low x_{Bj} DIS, the exciting prospect of a new quantitative understanding of the bulk of soft hadronic physics in terms of QCD may be possible. That indeed would be a major step forward in our understanding of hadronic interactions.

8. Deep–Inelastic *ep* Physics: Diffraction

8.1. The Leading Rapidity Gap Phenomenon in DIS

Following the ZEUS experiment [46], DIS ep events were reported in 1993 [47, 48] by H1 in which a leading "rapidity gap" phenomenon was observed in the forward direction (see figure 1 for examples of DIS events with and without a forward rapidity gap). In a search for intervals of laboratory pseudo–rapidity which are devoid of hadronic energy ($E_{had} < 400\,\mathrm{MeV}$ at the finest "cell" level of LAr segmentation), a scatter plot (figure 16) of the largest such interval $\Delta\eta$ against the pseudo–rapidity of the forward end of $\Delta\eta$ in the LAr demonstrates that

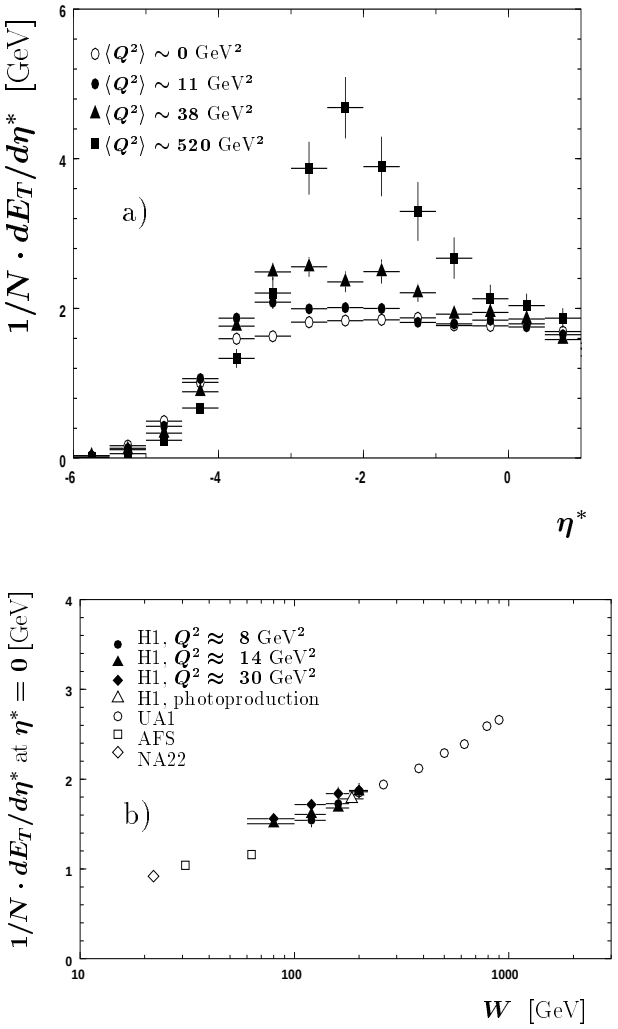

Figure 15. a) Transverse energy flow $\frac{1}{\eta^*}\frac{\mathrm{d}E_T}{\mathrm{d}\eta^*}$ in $\gamma^* p$ interactions (for $0.3 \leq y \leq 0.7$) as a function of pseudo–rapidity η^* in the $\gamma^* p$ CMS; b) transverse energy flow in the central region $\eta^* = 0$ as a function of W for different Q^2; also shown in b) are measurements from the central region ($\eta^* = 0$) in pp inelastic collisions (UA1, AFS, NA22) at the same W.

the leading effect is empty intervals adjacent to the most forward acceptance ($\eta = 3.65$). Such events were anticipated [49, 50] as the manifestation of diffractive $\gamma^* p$ physics.

Much can be inferred from the simple observation in H1 of such "rapidity gaps". Any such phenomenon in which the distribution of gap size is not exponentially suppressed in the overall CM ($\gamma^* p$) frame has been taken by Feynman and Bjorken [50, 51] as the definition of a diffractive phenomenon. In figure 17 is shown the distribution of η^*_{max}, the most forward pseudo–rapidity in the $\gamma^* p$ CM frame (where as in the laboratory frame the incident proton direction specifies positive η^*) of any hadronic energy in the LAr. If the rapidity gap implied by the measurement of η^*_{max},

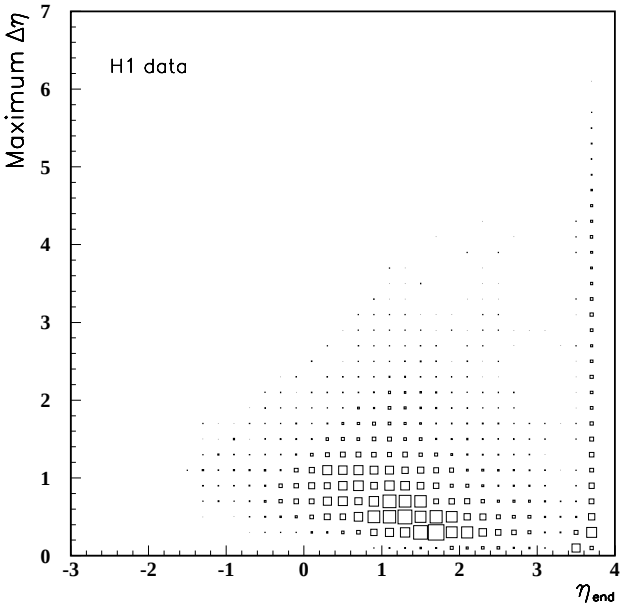

Figure 16. For all ep DIS candidate events, scatter plot of the forward end η_{end} of the largest laboratory pseudo–rapidity interval $\Delta\eta$ which is devoid of hadronic energy in the LAr against $\Delta\eta$; a distinct class of events with a tail to large $\Delta\eta$ and with an interval ending at the end of the acceptance of the LAr ($\eta = 3.65$) is visible.

extends right to the forward proton direction, then the lack of any dependence ("exponential suppression") amounts to a diffractive proton interaction à la Bjorken. The interpretation is that there is a colourless momentum transfer coupling to the incident proton in the DIS ep interaction because of the lack of any significant hadronic energy in the rapidity gap (figure 18). Assuming the Bjorken criteria, this colourless momentum transfer corresponds to that in diffraction, which is usually discussed in terms of the exchange of a pomeron ($I\!P$) in the parlance of soft hadronic physics. We have a deep–inelastic diffractive $\gamma^* p$ interaction in which the proton scatters or dissociates, leaving itself or most of its dissociation products in the beam pipe. Both cases, proton scattering or proton dissociation, can sometimes be conveniently distinguished from "standard" ep DIS by referring to diffraction as DIS with a "colourless proton remnant" (hereafter written R_c).

8.2. The Contribution of Diffraction to Deep–Inelastic ep Scattering

To proceed further requires a more quantitative approach, and this has been achieved in H1 by evaluating the contribution to the proton structure function F_2 of interactions with colourless exchange coupling to the incident proton. A sample of events

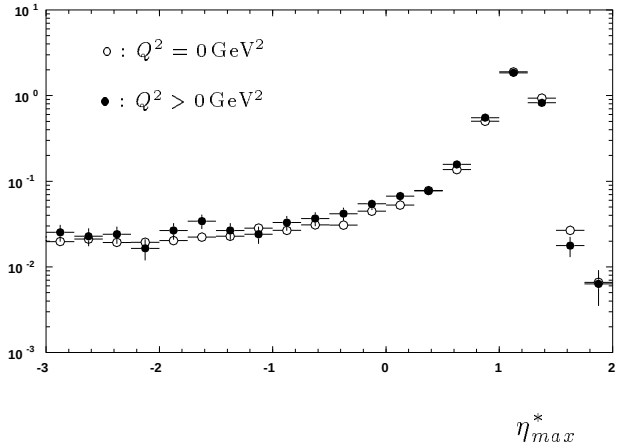

Figure 17. Distribution of maximum pseudo–rapidity η^*_{max} for both ep DIS events (filled points) and ep photoproduction events (open points) in the $\gamma * p$ CM system; the plateau with no exponential suppression corresponding to diffractive interactions is clearly visible in both.

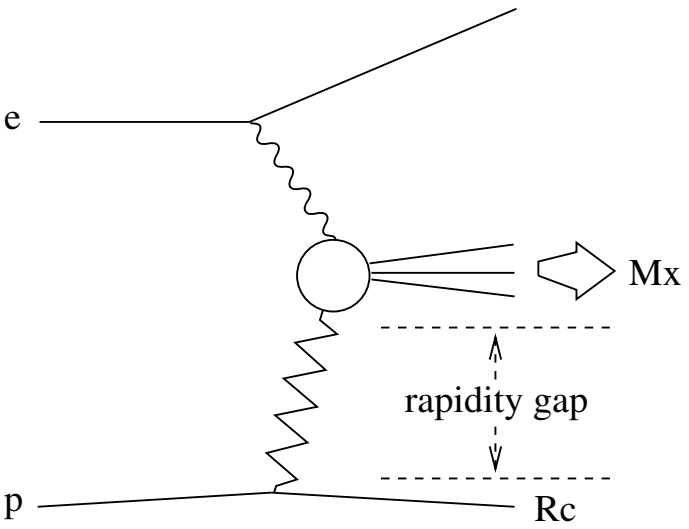

Figure 18. Schematic "Feynman" diagram of a deep–inelastic ep interaction in which there is a forward diffractive "rapidity gap" devoid of hadronic energy; the high Q^2 probing virtual proton interacts with a colourless entity associated with the target proton.

in which such a mechanism is likely to predominate is obtained by requiring the presence of a rapidity gap adjacent to the remnant R_c.

The procedure starts with the definition of the quantity to be measured as $F_2^{D(3)}$, which, anticipating the results, is called the "diffractive structure function" following the original procedure of [52, 53]. The measurement of $F_2^{D(3)}$ is made as a function of the three kinematic variables β, Q^2, and x_{Bj}, or equivalently β, Q^2, and $x_{I\!P} = x_S$ (see section 2). In direct analogy with the definition of F_2 (equation 4) $F_2^{D(3)}$ is evaluated assuming

$$\frac{\mathrm{d}^3\sigma^{ep\to eXR_c}}{\mathrm{d}x\mathrm{d}Q^2\mathrm{d}x_{I\!P}} = \frac{4\pi\alpha^2}{xQ^4}\left\{1 - y + \frac{y^2}{2}\right\} F_2^{D(3)}(x, Q^2, x_{I\!P})$$

where there is an implicit integration of the ep DIS cross section $\frac{\mathrm{d}^4\sigma^{ep\to eXR_c}}{\mathrm{d}x\mathrm{d}Q^2\mathrm{d}x_{I\!P}\mathrm{d}t}$ for the process $ep \to eXR_c$ over the unmeasured quantity t, the 4–momentum transfer squared at the incident proton vertex, and where the sensitivity to the longitudinal to transverse virtual photon cross section ratio $\sigma^{\gamma^*_L p\to XR_c}/\sigma^{\gamma^*_T p\to XR_c}$ for rapidity gap dynamics is ignored because its effect is small at the present level of experimental precision. These, and other details, are all discussed in [54].

In terms of the discussion of deep–inelastic kinematics in section 2, the distribution of invariant mass constituting W is here compartmentalised nicely in terms of M_X, which is measured in each event as the invariant mass in LAr to the start of the forward rapidity gap (η_{max}), and the rest, which is associated with the proton remnant R_c in the deep–inelastic process $ep \to eXR_c$ and which is mostly outside the acceptance of the experiment (inside the beam pipe). In terms of this M_X, x_S (section 2) becomes the fraction of the incident proton 4–momentum P carried in the colourless exchange, assumed to be a low $|\,t\,|$ phenomenon. Thus by requiring that DIS events have an η_{max}, an event sample is obtained both for which colour isolation between R_c and the deep–inelastic fragments is most likely to be present, and for which a well defined mass M_X is specified. The process, whose cross section is measured and then quoted in the form of $F_2^{D(3)}$, corresponds to $ep \to eXR_c$, where the (undetected) colourless proton remnant R_c has 4–vector P_{R_c} which is related to that of the proton P according to $P_{R_c} = (1 - x_{I\!P}) \cdot P$, and for which $|t| \lesssim 7\,\mathrm{GeV}^2$.

The contribution $F_2^{D(3)}$to F_2 attributable to colourless exchange with the proton is then evaluated from the data using events for which a forward rapidity gap, that is an η_{max} cut, can be established. Figure 19a) shows the η_{max} spectrum measured using the LAr energy clusters of all ep DIS data. A "non–exponentially suppressed tail", now in the colinear ep set of reference frames, extending away from the forward direction is clear. The expectation from simulations [34, 35] of ep DIS which do not include any such colourless exchange clearly fails to account for this tail.

In the H1 analysis the forward detectors PLUG ($3.54 < \eta < 5.08$) and FMD ($5.0 < \eta < 6.6$) play a crucial role because they cover the region where hadron production is most likely to be depleted for colourless momentum transfer coupling to the proton [5]. As a result they permit a sample of events to be selected with $\eta_{max} = 3.2$ so that almost all of the acceptance of LAr ($\eta \leq 3.65$) is available for subsequent physics

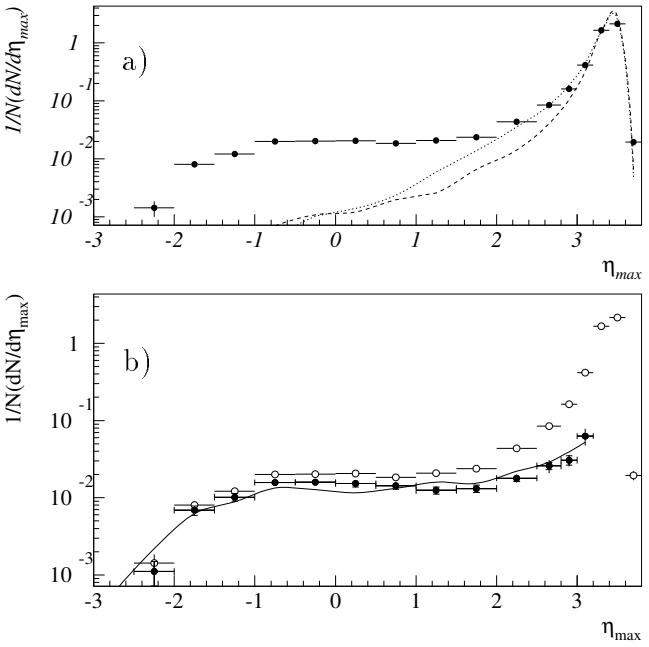

Figure 19. Distribution of maximum pseudo–rapidity η_{max} for ep DIS events; the excess at smaller η_{max} is clearly visible; also shown in a) are the expectations from two "standard DIS" simulations (CDM and MEPS) in which the probing virtual photon couples directly with a quark in the proton; also shown in b) is the η_{max} spectrum of the final data used to evaluate $F_2^{D(3)}$together with the expectation from a diffractive deep–inelastic simulation RAPGAP.

analysis. This has two very important consequences for the measurement of $F_2^{D(3)}$. The number of events with a well defined M_X is maximised, and almost the full kinematic range in M_X which can be measured with LAr is available. In figure 19b) the η_{max} distribution is shown for the final sample of putative diffractive events extending to $\eta = 3.2$, together with the expectation of a diffractive DIS simulation [55].

A problem, which is common to all analyses of this type, is the definition at larger η_{max} values (corresponding to larger M_X and $x_{I\!P}$ values) of the contribution due to "standard DIS" events in which a rapidity gap occurs in the normal course of statistical fluctuation in parton hadronisation. In the H1 analysis, this contribution is estimated conservatively as a function of β, Q^2, and $x_{I\!P}$ using the two very different simulations CDM and MEPS (see figure 19), and for the results presented here this contribution is not included in $F_2^{D(3)}$. Measurements of $F_2^{D(3)}$for which it exceeds 25% are always rejected. The analysis is repeated for a variety of different cuts in η_{max}, including none whatsoever! Apart from changing somewhat the kinematic range accessible, the results are always completely consistent, measured point by measured point, to well within final errors.

The results for $F_2^{D(3)}$are summarised in figure 20.

8.3. The Identification of and Characteristics of Diffraction in Deep–Inelastic Scattering

Everywhere $F_2^{D(3)}$ is observed to decrease monotonically with increasing $x_{I\!P}$ in the measured range $3 \times 10^{-4} \leq x_{I\!P} < 0.05$. An excellent fit to all data points, irrespective of β and Q^2, is obtained assuming a polynomial dependence $x_{I\!P}^{-n}$ with a single exponent $n = 1.19 \pm 0.06(stat.) \pm 0.07(syst.)$, χ^2/d.f. = 32.0/46, 94% C.L. (χ^2/d.f. = 64.5/46, 4% C.L. assuming only statistical errors). The observed universal dependence on $x_{I\!P}$ is thus a feature of the measurements at the level of statistical accuracy. There is no evidence for any systematic trend in the contributions to χ^2 as a function of β and Q^2.

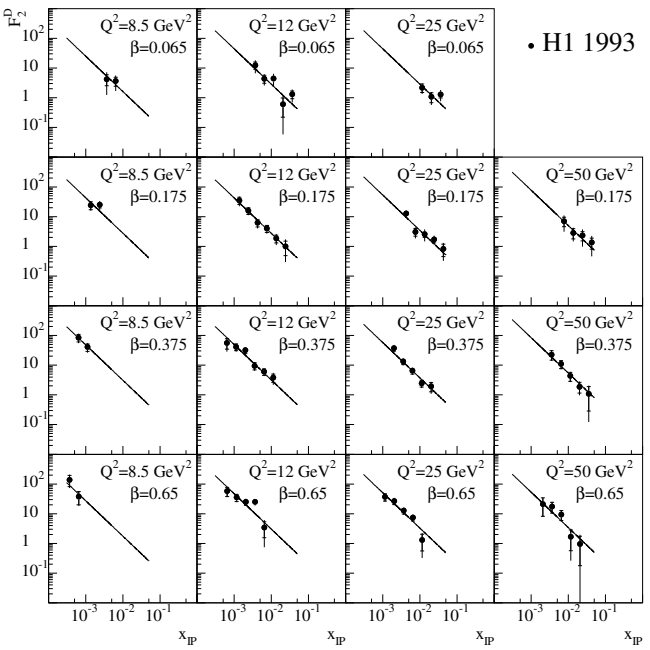

Figure 20. The diffractive contribution $F_2^{D(3)}(\beta, Q^2, x_{I\!P})$ to the proton structure function F_2 as a function of $x_{I\!P}$ for different β and Q^2; the inner error bar is the statistical error; the full error shows the statistical and systematic error added in quadrature; superimposed is the result of the fit establishing a factorisable dependence of the form $\propto x_{I\!P}^{-n}$ (see text). Note that an overall normalisation uncertainty of 8% is not included.

Such a universal dependence on $x_{I\!P}$, independent of β and Q^2, is expected naively if the deep–inelastic process responsible for rapidity gap events involves a (colourless) target T in the incident proton whose characteristics are not dependent on $x_{I\!P}$, and which carries only a small fraction of the proton's momentum. The dependence of $F_2^{D(3)}(\beta, Q^2, x_{I\!P})$ then factorises into the product of a universal term ($f_{T/p}(x_{I\!P}) \propto x_{I\!P}^{-n}$), which describes the "flux" of T "in" the proton, and

a term which describes any structure of T and which is a function of only β and Q^2. The electron scattering cross section for the process $ep \to eXR_c$ can then be written

$$\frac{\mathrm{d}^3\sigma_{ep\to eXR_c}}{\mathrm{d}\beta \mathrm{d}Q^2 dx_{I\!P}} = \frac{\mathrm{d}^2\sigma_{eT\to eX}}{\mathrm{d}\beta \mathrm{d}Q^2} \cdot f_{T/p}(x_{I\!P})$$

where $\frac{\mathrm{d}^2\sigma_{eT\to eX}}{\mathrm{d}\beta \mathrm{d}Q^2}$ describes the deep–inelastic scattering of the electron off T.

The interpretation of the colourless component T of the proton follows from the phenomenology of hadronic physics and the shibboleth of the $I\!P$. If T is taken to be well parameterised in terms of "Reggeised" hadronic exchanges, then the $x_{I\!P}$ dependence of the flux factor is specified by the leading Regge trajectory $\alpha(t)$ in the "asymptotic limit" $x_{I\!P} \to 0$, $t/s \to 0$. The dependence takes the form $x_{I\!P}^{-[2\alpha(t)-1]}$ [56, 57, 58]. In this measurement we perforce integrate over t. To good approximation, $\alpha(t)$ may be replaced by $\alpha_{t=0}$ because the t distribution of the soft hadronic proton interaction is likely to be "peripheral" and the t dependence of $\alpha(t)$ is likely to be slight.

The observed $x_{I\!P}$ dependence is consistent with the leading (effective) trajectory which describes phenomenologically "soft hadronic" diffractive interactions, namely the $I\!P$ with $\alpha(t) = \alpha_{t=0} + \alpha' t$ and $\alpha_{t=0} = 1.085$, $\alpha' = 0.25\,\mathrm{GeV}^{-2}$ [59]. The colourless proton remnant R_c is then either a proton or an isospin $\frac{1}{2}$ baryon excitation (eg N^*, $N^*\pi$, etc). If the t distribution of proton diffraction is here like that in soft pp collisions, namely peripheral with a dependence e^{bt} with $b \gg 1$, then the systematic error, which arises by ignoring any t dependence of $\alpha(t)$ of size given by the slope $\alpha' = 0.25\,\mathrm{GeV}^{-2}$ of the $I\!P$ trajectory and taking $n = 2\alpha_{t=0} - 1$, is ~ 4 to 5%. Note that the leading meson Regge trajectories, the $f_2(1270)/\omega(783)$ for a diffractive–like process with no isospin exchange, and the exchange degenerate $\rho(770)/a_2(1320)$ for a process involving isospin exchange, have intercept $\alpha_{t=0} \sim 0.5$, giving rise to an $x_{I\!P}$ dependence which is much less steep. Parameterisations of pion exchange, either "Reggeised" ($\alpha_{t=0} \sim 0$) or otherwise, have only a slight dependence on $x_{I\!P}$. Therefore the interpretation of the rapidity gap events in DIS at low Bjorken–x as being due in the main either to diffractive scattering or to diffractive dissociation of the incident proton can be made without ambiguity.

In calculations which use the BFKL QCD formalism of $I\!P$ dynamics, the $I\!P$ is found to be "hard" with an intercept $\alpha_{t=0} = 1 + \varepsilon$, $\varepsilon \lesssim 0.5$ [60, 18]. Combining in quadrature the statistical and systematic errors of the measurement of the $x_{I\!P}$ dependence above, the intercept cannot exceed 1.25 (i.e. $\varepsilon \leq 0.25$) with 99.85% confidence, if the effects of t dependence are ignored. The simplest, but debatable, assumption (based as above on a trajectory slope $\alpha' = 0.25\,\mathrm{GeV}^{-2}$) concerning t dependence *could* raise this upper limit by between 0.04 and 0.05. Thus this measurement does not rule out such a "hard" $I\!P$, especially if it contributes together with a soft component, such as that described above. A recent calculation, based on a BFKL approach, suggests also that the simplest factorisation with an $x_{I\!P}$ dependence $\propto x_{I\!P}^{-n}$ may not strictly hold [61]. The accuracy of this measurement of the $x_{I\!P}$ dependence does not exclude such a possibility.

8.4. The Partonic Structure of Proton Diffraction

The observation that rapidity gap events in DIS are dominantly of a diffractive nature, and the evidence for a simple factorisation of the structure function $F_2^{D(3)}(\beta, Q^2, x_{I\!P})$ lead naturally to the interpretation of the β and Q^2 dependence of $F_2^{D(3)}$ as a measure of the deep–inelastic structure of diffractive exchange. If such exchange is taken phenomenologically to be described by an effective Regge trajectory, this interpretation amounts to the deep–inelastic structure of the $I\!P$.

In figure 21 are shown the β and Q^2 dependences of the integral

$$\tilde{F}_2^D(\beta, Q^2) = \int_{x_{I\!P_L}}^{x_{I\!P_H}} F_2^{D(3)}(\beta, Q^2, x_{I\!P})\,\mathrm{d}x_{I\!P},$$

which, assuming factorisation, is proportional to the structure function of the $I\!P$. The range of integration, $x_{I\!P_L} = 3 \times 10^{-4}$ and $x_{I\!P_H} = 0.05$ is chosen to span the entire $x_{I\!P}$ range of measurements of $F_2^{D(3)}$. $\tilde{F}_2^D$ is evaluated assuming that the factorisation hypothesis with the measured dependence on $x_{I\!P}$ is a good description over this range of integration. It is convenient to define $\tilde{F}_2^D(\beta, Q^2)$ in this way to avoid the need to specify the normalisation of the unknown diffractive, or $I\!P$, "flux" in the proton when presenting the data in a form which is suitable for direct comparison with theoretical expectation for $I\!P$ structure.

There is no evidence for any substantial Q^2 dependence of $\tilde{F}_2^D$ for any β. Deep (high Q^2) diffractive interactions are thus broadly of a scale invariant, and therefore point-like, nature. Furthermore, $\tilde{F}_2^D$ is observed to have little dependence on β with contributions throughout the measured range ($0.065 < \beta < 0.65$). Therefore the structure which is resolved by the electron in the high Q^2 diffractive interaction carries only a fraction of the $I\!P$'s momentum, implying that the $I\!P$ has its own point-like, presumably partonic, sub–structure.

A fit to the hypothesis of a linear $\log_{10} Q^2$ dependence of the form

$$\tilde{F}_2^D(\beta, Q^2) = a(\beta) \log_{10} Q^2 + b(\beta) \qquad (5)$$

yields values for $a(\beta)$ that are $\simeq 1.5\sigma$ above zero for all values of β. The errors in $a(\beta)$ amount to $\sigma =$

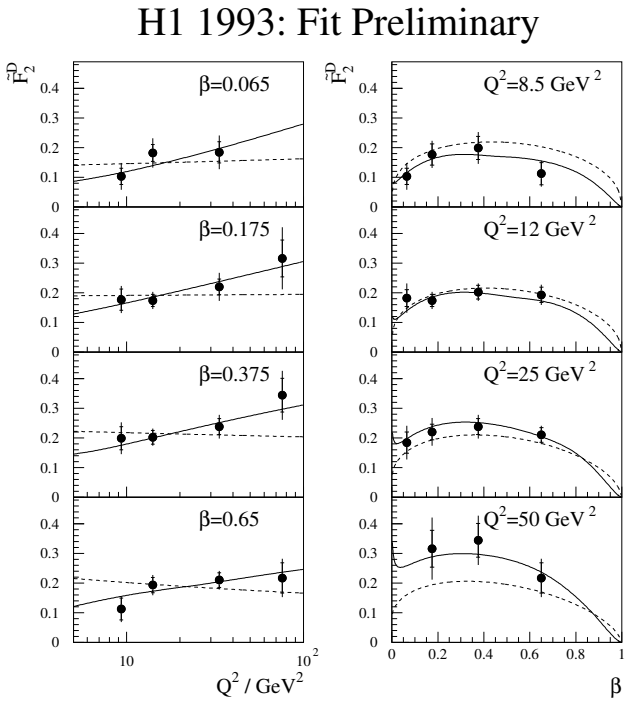

Figure 21. Dependence of $\tilde{F}_2^D$ on Q^2 and β; superimposed are the results of two LO $\log Q^2$ DGLAP QCD fits. The dashed line shows a fit in which at the starting scale, $Q_0^2 = 4\,\mathrm{GeV}^2$, diffraction is attributed to the exchange of only quarks (χ^2/dof of 13/12, 37%C.L.). The solid line shows a fit in which both quarks and gluons may contribute to the diffractive mechanism at $Q_0^2 = 4\,\mathrm{GeV}^2$ (χ^2/dof = 4/9, 91%C.L.). In the latter, the gluons carry $\sim 90\%$ of the momentum of the pomeron at $Q_0^2 = 4\,\mathrm{GeV}^2$.

$0.09\,(\log_{10}\mathrm{GeV}^2)^{-1}$ for all β except that at $\beta = 0.065$ for which $\sigma = 0.15\,(\log_{10}\mathrm{GeV}^2)^{-1}$. Therefore the accuracy of this first measurement of the Q^2 dependence of $\tilde{F}_2^D$ is such that the possibility of "scaling violations", symptomatic of QCD, may be admitted.

The hypothesis that any violation of scale invariance is in the form of a $\log Q^2$ dependence of $\tilde{F}_2^D$ which is independent of β (slope parameter a in equation 5 now independent of β) provides an excellent description of $\tilde{F}_2^D$ and gives $a = 0.14 \pm 0.04$. In this and all subsequent fits below, statistical and systematic errors are added in quadrature.

The lack of any fall of $\tilde{F}_2^D$ with increasing Q^2 at large β contrasts with the violations of scale invariance exhibited by the structure function of a typical hadron. For example, the proton structure function F_2 rises with increasing Q^2 for $x \lesssim 0.15$, and falls with increasing Q^2 for $x \gtrsim 0.15$ [27, 28]. This decreasing dependence at high x is an inevitable consequence of DGLAP QCD evolution for an object with a structure built from the evolution of "valence" quarks in which the latter predominate at large Bjorken–x. By analogy, a structure function for which any violation of scale invariance amounts to an increase with $\log Q^2$ at high Bjorken–x (β), is likely to have a large gluon, relative to quark, content in its valence parton density. The observation that the Q^2 dependence of $\tilde{F}_2^D$ is consistent with a rise proportional to $\log Q^2$ thus suggests that a significant contribution to the structure of diffractive exchange is gluonic.

To quantify any substantive evidence for a gluonic contribution to the structure of diffractive exchange, that is to $\tilde{F}_2^D$, the DGLAP evolution equations were solved numerically in LO and in NLO $\log Q^2$ approximations. The numerical technique used followed that of [62] in which, starting from a scale $Q_0^2 = 4\,\mathrm{GeV}^2$, the assumed forms $z^a(1-z)^b$ for the gluon and flavour singlet quark parton densities ($z = x_{i/I\!P}$, quark $i = q$, gluon $i = g$) in diffractive exchange were evolved to higher Q^2 and compared with the measurements of the β dependence of $\tilde{F}_2^D$. The basic kinematic features of the method, for example the treatment of charm, were identical to those in the QCD analysis of the proton structure function F_2 [26]. More details can be found in [63]. In particular, no momentum sum rule was imposed because it is far from clear whether one should exist for such a space–like exchange, and because the normalisation of $\tilde{F}_2^D$ does not coincide with the normalisation of the structure function of diffractive exchange without further theoretical input.

The results of the QCD analysis (figure 21) are only indicative because of the limited precision of this first measurement of $F_2^{D(3)}$(see Phillips [63]). Nevertheless a picture begins to emerge which confirms the qualititative statements above concerning the $\log Q^2$ dependence at higher β. The measurements favour the presence of a significant gluon contribution (usually between about 70 to 90%) of the form $zg(z) = z^8(1-z)^{0.3}$ ($z = x_{g/I\!P}$) at the starting scale $Q_0^2 = 4\,\mathrm{GeV}^2$ if they are not to exhibit a falling $\log Q^2$ dependence at high β (91% CL). Taking only quarks at $Q_0^2 = 4\,\mathrm{GeV}^2$ with a similar pdf dependence $zq(z) = z^{0.35}(1-z)^{0.35}$ ($z = x_{q/I\!P}$), though acceptable quantitatively (37% CL), does not reproduce this striking feature in the data. Furthermore, and with marginal significance, the favoured gluon distribution in diffractive exchange has the leading form above in which the majority of the diffractive 4–momentum transfer is taken by a single gluon, that is $I\!P$ exchange involves a leading gluon exchange (figure 22).

The observation above that the scaling violations of $\tilde{F}_2^D$ are consistent at the present rather limited level of experimental precision with the form of equation 5 with $a(\beta)$ constant is reminiscent of the dependence of the structure function F_2^γ of the photon [16, 12, 13]. There the observed scaling violations are observed to be consistent with QCD expectation driven by the so–called "inhomogeneous" term which corresponds to the leading "point-like" coupling of the photon to

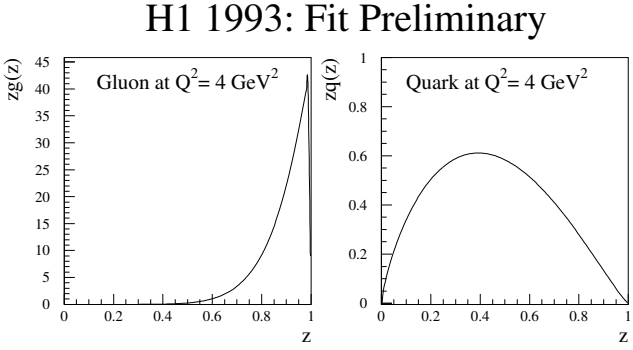

Figure 22. The quark flavour–singlet $zq(z)$ and the gluon $zg(z)$ densities at the starting scale $Q_0^2 = 4\,\mathrm{GeV}^2$ in the LO QCD description of $\tilde{F_2^D}$ which describes the well the tendency for a rise with increasing $\log Q^2$ at high β by means of a leading gluon density. The gluons account for $\sim 90\%$ of the total momentum in diffractive exchange. The normalisation is taken from the measurement of $\tilde{F_2^D}$ which itself is proportional to the structure function of diffractive exchange. The statistical preference for this solution is slight, a symmetric dependence $zg(z) = z(1-z)$ for example being consistent overall with the measurement of $\tilde{F_2^D}$ but failing to describe the tendency of the data to rise with increasing $\log Q^2$ at $\beta = 0.65$.

$q\bar{q}$ [64]. Furthermore, such a leading "point–like" coupling has a dependence on the appropriate Bjorken–x like variable which persists to large values by virtue of the $\gamma \rightarrow q\bar{q}$ splitting function $P_{q/\gamma} \propto z^2 + (1-z)^2$ contribution to F_2^γ. The similarity of F_2^γ with the observed Q^2 and β dependences of $\tilde{F}_2^D$ is striking. The intriguing possibility therefore exists that, like the photon, diffractive exchange ($I\!P$) has such an inhomogeneous, and therefore point–like, contribution to its structure function. In view of the same z dependences of the splitting functions $\gamma \rightarrow q\bar{q}$ and $g \rightarrow q\bar{q}$, this point–like contribution may naturally be attributed to a gluon. If it is, then any distinction between such a possibility and the more straightforward consequences described above of the application of DGLAP, which seem to show some suggestion of a leading gluon, is unclear. If it is not, then we have something in diffractive exchange which is point–like and which is completely new!

8.5. A Parton Model Approach to DIS Rapidity Gap Physics

Diffraction in terms of $I\!P$ exchange requires a certain faith in the interpretation of the energy dependence of hadronic physics cross sections in terms of a leading effective Regge pole. An attempt has been made by Buchmüller and Hebecker [65] to develop a partonic model of DIS ep events with a rapidity gap without the assumption of any diffractive paradigm, and with the assumption that the underlying partonic process is electron–gluon scattering. The motivation is derived from the importance of such dynamics in low–x_{Bj} deep–inelastic ep scattering, and by implication therefore it requires diffractive exchange to be predominantly a leading gluon phenomenon. It is hypothesised that the quark–antiquark pair produced in the hard electron–gluon interaction undergoes colour rotation so that the colour quantum numbers of the initial quark–antiquark system are completely randomised. Then the probabilities of obtaining a colour singlet or octet configuration in the final state are simply $\frac{1}{9}$ and $\frac{8}{9}$ respectively. When the quark–antiquark pair emerge in a colour singlet state, there is no longer any colour connection between it and the proton remnant, and so a "rapidity gap" is likely.

The approach leads to a simple, parameter free, prediction for the relationship between the structure functions $F_2(x_{Bj}, Q^2)$ and $F_2^{D(3)}$. A simple scaling law of the form

$$\xi F_2^{D(3)}(\beta, Q^2, x_{I\!P} = \xi) \propto F_2(x_{Bj} = \xi, Q^2)$$

is predicted which should hold for any β to the extent that the model predicts little or no β dependence of $F_2^{D(3)}$. This prediction is shown to be broadly correct in figure 23 in which the measurements of $F_2^{D(3)}$for different β are included together with the measurements of $\frac{F_2(x_{Bj})}{x_{Bj}}$ multiplied by a factor 0.04. This factor corresponds to the proportion overall of deep–inelastic diffraction being $\frac{1}{9}$, following the colour rotation assumption in [65].

The measurement of $F_2^{D(3)}$has been used to measure the total contribution of diffraction to F_2 as a function of x_{Bj} and Q^2 and thereby to demonstrate explicitly the prediction of the relative normalisations of F_2 and $F_2^{D(3)}$. Diffraction is defined to be for $x_{Bj} \leq x_{I\!P} \leq 0.05$ so that the contribution can be expressed as $F_2^D(x_{Bj}, Q^2)$ which is related to $F_2^{D(3)}$according to

$$F_2^D(x_{Bj}, Q^2) = \int_x^{0.05} F_2^{D(3)}(x_{Bj}, Q^2, x_{I\!P})\mathrm{d}x_{I\!P} \qquad (6)$$

The results are shown in figure 24 both as $F_2^D(x_{Bj}, Q^2)$ and as the proportion $r^D(x_{Bj}, Q^2) = F_2^D/F_2$. Note that both F_2^D and r^D tend to zero as $x_{Bj} \rightarrow x_{I\!P}$. Away from this kinematic limit, r^D is rather insensitive to x_{Bj} and Q^2 and is about 10%. The prediction based on colour rotation in [65] that $r^D = \frac{1}{9}$ is thus shown to be consistent with measurement, albeit with the definition of diffraction implicit in equation 6 above, namely $x_{Bj} \leq x_{I\!P} \leq 0.05$.

The approach of Buchmüller and Hebecker [65] is thus in remarkable agreement with experiment, given the simplicity of this first model calculation. It adds weight to the picture in which diffractive exchange, and thus the $I\!P$, is a leading gluon phenomenon.

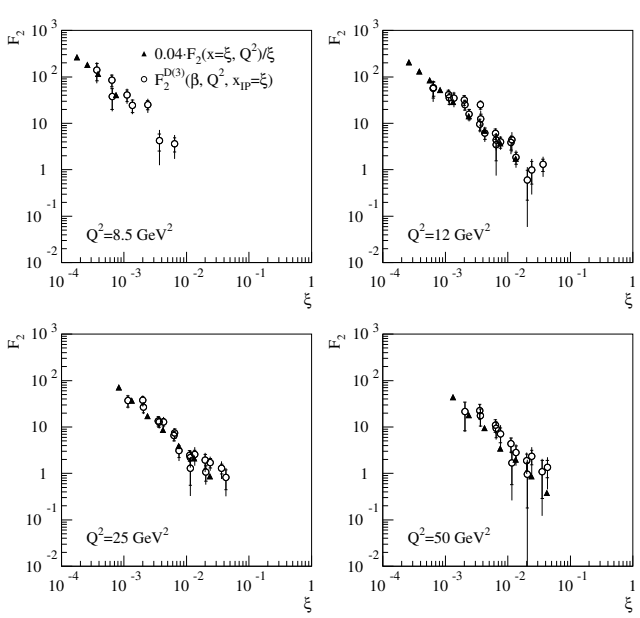

Figure 23. The quantities $F_2^{D(3)}(\beta, Q^2, x_{I\!P} = \xi)$ and $0.04 \cdot F_2(x = \xi, Q^2)/\xi$ as a function of ξ for different values of Q^2 to test the scaling law of Buchmüller et al. (see text); note that the $F_2^{D(3)}$ are plotted in each plot for different β.

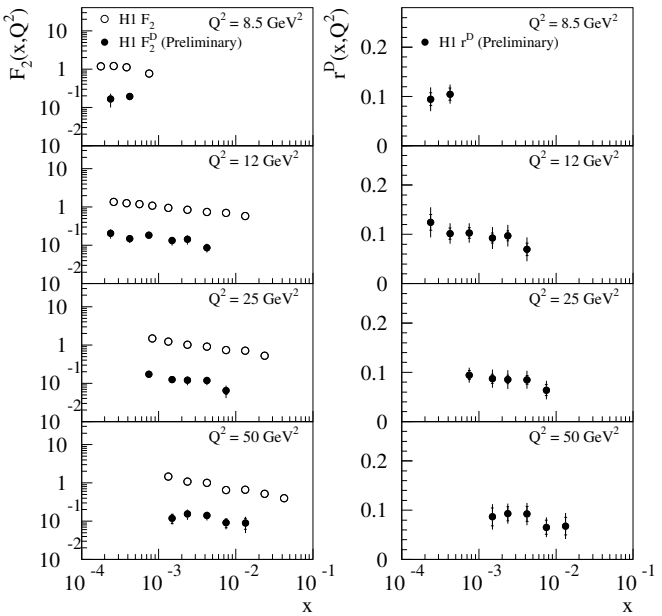

Figure 24. The structure function $F_2^D(x_{Bj}, Q^2)$ and the ratio $r^D = F_2^D(x_{Bj}, Q^2)/F_2(x_{Bj}, Q^2)$ for $x_{I\!P} < 0.05$; the result is for deep–inelastic diffraction in which the proton does not dissociate; about a third of deep–inelastic diffractive interactions are consistent with proton dissociation.

8.6. Summary

Remarkable progress has been made in our understanding of rapidity gap phenomena in ep DIS since the last DIS Workshop in 1994 at Eilat, Israel, where the first mention of the "Bartels Gap" between experiment and theory was heard [66]. Following quantification in terms of a diffractive structure function $F_2^{D(3)}$, rapidity gap events in ep DIS are now unquestionably attributable to diffractive interactions and amount to roughly 10% of low x ep DIS, irrespective of $x\,(\ll x_{I\!P})$ and Q^2. To within present experimental uncertainty, the characteristics of the colourless exchange are universal and follow the broad expectation encapsulated in $I\!P$ phenomenology of hadronic diffraction. The deep–inelastic evolution of $F_2^{D(3)}$ is readily interpreted in terms of diffraction as a leading gluon phenomenon in QCD.

The next year should see experimental precision improve to the extent that the precise nature of diffractive deep–inelastic dynamics may become established, in particular whether there is real evidence for a "hard" perturbative $I\!P$, anticipated for so long in QCD.

Looking further into the future is yet more exciting. These measurements at HERA, both in H1 and ZEUS, amount to the first opportunity to measure the partonic structure of soft, long range, hadron–hadron interactions, and thereby to gain insight into the stability or otherwise of both putative and established hadronic systems. The feasibility at HERA of measuring the structure functions of hadronic momentum transfer, as well as of hadrons themselves, could have significant impact on one of the oldest questions in 20th century physics – how do two protons interact? – and thus ultimately, why is matter the way that it is?

9. Conclusion

Time has permitted only a soupçon of the rich panoply of deep–inelastic physics with H1 at HERA to be presented. There is little point in again listing the topics covered. Ignored, with no intention whatsoever of any sleight to colleagues in the H1 collaboration, have been new measurements of charged current physics [67], continuing searches for evidence of supersymmetry, lepton excitation and leptoquark production [68], precision measurements of the decomposition of the total hadronic photoproduction cross section in terms of elastic, single and double dissociative photon diffraction [7], and heavy flavour physics.

The choice of topics to which attention has been drawn has been guided by the classic motivation of any high energy lepton–nucleon experiment, namely the elucidation of the short distance structure of matter. Great steps forward have already been taken with the electron microscope that is HERA plus H1. The partonic structure of the photon is being further revealed, the low x structure of the proton has been measured for the first time, and the first measurements

of the QCD structure of the dominant soft hadronic interaction mechanism, diffraction, have been made.

None of the results discussed here are based on the operation of HERA at peak luminosities greater than about $4.3 \times 10^{30}\,\mathrm{cm}^{-2}\,\mathrm{s}^{-1}$. As the unique challenges posed by the operation of HERA, the world's first collider of different particle species, continue to be met and the operational luminosity and duty cycle improve further, the outlook for ep physics remains as exciting as ever.

Acknowledgements

Je remercie V. Brisson et tous les organisateurs d'un DIS95 Workshop très intéressant et de l'opportunité pour un séjour très agréable au printemps à Paris.

None of the physics presented here would have been possible without the immense efforts of very many people. The operation of HERA is due to the dedication and skill of the few who constitute the machine groups at DESY. The construction and operation of H1 is due to similar dedication, skill and determination of technicians and engineers in all the H1 collaborating institutes since 1986. The on–going operation, data taking, and data analysis work is in the expert hands of all my colleagues in H1, with whom it is always a pleasure to work. The support of the UK Particle Physics and Astronomy Research Council is gratefully acknowledged. I thank the DESY laboratory for their hospitality, and the University of Liverpool for maintaining its belief in the merits of a strong and well funded Department of Physics. Without the hard work, persistence, enthusiasm and originality of two colleagues, A. Mehta and J. Phillips, much of the diffractive physics reported above would be only fantasy. J. Bartels, W. Buchmüller, A. Donnachie, A. Hebecker, G. Ingelman, G. Kramer, P. Landshoff, N. Nikolaev and W. J. Stirling have patiently tolerated my ignorance of the theoretical details of hadronic diffraction and QCD, and thereby influenced the presentation of the experimental results on this topic. I also thank A. De Roeck for correcting a couple of my misunderstandings concerned with proton structure function physics and low x QCD.

References

[1] I. Abt et al. (H1 Collaboration), "The H1 Detector at HERA", DESY preprint DESY 93-103 (1993).
[2] B. Andrieu et al. (The H1 Calorimeter Group), Nucl. Inst. Meth. **A336** (1993) 460.
[3] B. Andrieu et al. (The H1 Calorimeter Group), Nucl. Inst. Meth. **A336** (1993) 499.
[4] H. I. Cronström et al. Nucl. Inst. Meth. **A340** (1994) 304.
[5] A. Mehta, "Measurement of the Diffractive Proton Structure Function and Calibration of the Forward Muon Detector at H1", PhD thesis (University of Manchester), 1994 (unpublished) and Rutherford Appleton Laboratory report RALT-037.
[6] E. J. Williams, Proc. Roy. Soc. London **A139** (1933) 163
C. F. Weizsäcker, Zeit. Phys. **88** (1934) 612.
[7] S. Aid et al. (H1 Collaboration), "Measurement of the Total Photon Proton Cross section and its Decomposition at 200 GeV Centre of Mass Energy", DESY-95-162, accepted for publication in Zeit. Phys.
[8] A. Donnachie, P. V. Landshoff, Nucl. Phys. **B231** (1984) 189.
[9] H. Abramowicz, E. M. Levin, A. Levy, U. Maor, Phys. Lett. **B269** (1991) 465.
[10] T. Ahmed et al. (H1 Collaboration), Phys. Lett. **B314** (1993) 436
T. Ahmed et al. (H1 Collaboration), Nucl. Phys. **B445** (1995)195.
[11] G. Kramer, S. G. Salesch, Zeit. Phys. **C61** (1994) 277
D. Bobleker, G. Kramer and S. G. Salesch, Zeit. Phys. **C63** (1994) 471.
[12] H. Abramowicz, K. Charchula, A. Levy, Phys. Lett. **B269** (1991) 450.
[13] M. Glück, E. Reya and A. Vogt, Phys. Rev. **D46** (1992) 1973.
[14] M. Glück, E. Reya and A. Vogt, Zeit. Phys. **C53** (1992) 127
M. Glück, E. Reya and A. Vogt, Phys. Lett. **306B** (1993) 391.
[15] Yu. L. Dokshitzer, JETP **46** (1977) 641
V. N. Gribov and L. N. Lipatov, Sov. Journ. Nucl. Phys. **15** (1972) 78
G. Altarelli and G. Parisi, Nucl. Phys. **B126** 1977 298.
[16] Ch. Berger et al. (PLUTO Collaboration), Zeit. Phys. **C26** 353 (1984).
[17] G. Altarelli and G. Martinelli, Phys. Lett. **B76** (1978) 89.
[18] É. A. Kuraev, L. N. Lipatov, and V. S. Fadin, Sov. Phys. JETP **45** (1977) 199
Ya. Ya. Balitskiĭ and L. N. Lipatov, Sov. J. Nucl. Phys. **28** (1978) 822.
[19] A. H. Mueller and P. Navellet, Nucl. Phys. **B282** (1987) 727
[20] A. H. Mueller, Nucl. Phys. B (Proc. Suppl.) **18C** (1990) 125; J. Phys. **G17** (1991) 1443.
[21] T. Ahmed et al. (H1 Collaboration), Nucl. Phys. **B439** (1995) 471.
[22] G. Raedel, "New Results on the Proton Structure Function from H1", these proceedings.
[23] U. Bassler and G. Bernardi, "On the Kinematic Reconstruction of Deep Inelastic Scattering at HERA: the Sigma Method", DESY 94–231 (1994), submitted to Nucl. Instr. and Meth.
[24] A. De Roeck, J. Phys. **G19** (1993) 1549.
[25] T. Ahmed et al. (H1 Collaboration), Nucl. Phys. **B407** (1993) 515.
[26] T. Ahmed et al. (H1 Collaboration), Phys. Lett. **B354** (1995) 494.
[27] A. C. Benevenuti et al., Phys. Lett. **B223** (1989) 485; preprint CERN–EP/89-06.
[28] P. Amaudruz et al., Phys. Lett. **B295** (1992) 159; preprint CERN–EP/92-124.
[29] JADE Collaboration, W. Bartel et al., Zeit. Phys. **C33** (1986) 23.
[30] T. Ahmed et al. (H1 Collaboration), Phys. Lett. **B346** (1995) 415.
[31] Particle Data Group, Phys. Rev. **D50** (1994) 1173.
[32] T. Ahmed et al. (H1 Collaboration), Nucl. Phys. **B449** (1995) 3.
[33] New Muon Collaboration, D. Allasia et al., Phys. Lett. **B335** (1994) 220.
[34] G. Ingelman, "LEPTO 6.1", unpublished program manual, and in Proc. of the Workshop "Physics at HERA", 1366, ed. W. Buchmüller and G. Ingelman, Hamburg (1991)
H. Bengtsson, G. Ingelman and T. Sjöstrand, Nucl. Phys. **B301** (1988) 554.
[35] L. Lönnblad, Comput. Phys. Commun. **71** (1992) 15.
[36] I. Abt et al. (H1 Collaboration), Zeit. Phys. **C63** (1994) 377.

[37] J. Kwieciński, A. D. Martin, P. J. Sutton, K. Golec-Biernat, Phys. Rev. **D50** (1994) 217
K. Golec-Biernat, J. Kwieciński, A. D. Martin, P. J. Sutton, Phys. Lett. **B335** (1994) 220.
[38] I. Abt et al. (H1 Collaboration), Phys. Lett. **B356** (1995) 118.
[39] T. R. Ebert, "Hadronic Energy Flow in Deep Inelastic Electron-Proton Scattering and Proton Structure at low Bjorken x", PhD thesis (University of Liverpool), 1995 (unpublished) and Rutherford Appleton Laboratory report RALT-95-009.
[40] J. Kwieciński, A. D. Martin, P. J. Sutton, Phys. Rev. **D46** (1992) 921.
[41] J. Bartels, A. De Roeck, M. Loewe Z. Phys. **C54** (1992) 635
W. K. Tang, Phys. Lett. **B278** (1992) 363.
[42] A. De Roeck, "Forward Jets in Deep Inelastic Scattering at HERA", these proceedings.
[43] J. D. Bjorken and J. B. Kogut, Phys. Rev. **D8** (1973) 1341.
[44] S. Aid et al. (H1 Collaboration), "Comparison of Deep Inelastic Scattering with Photoproduction Interactions at HERA", DESY-95-156, accepted for publication in Phys Lett **B**.
[45] UA1 Collab., C. Albajar et. al., Nucl. Phys. **B335** (1990) 261
A. De Roeck, "Inclusive Particle Production in Hadronic Proton Interactions at 250 GeV", PhD thesis, Antwerpen (1988).
[46] M. Derrick et al. (ZEUS Collaboration) Phys. Lett. **B315** 481 (1993).
[47] W. Bartel, "$\sigma_{\gamma p}^{tot}$ and Diffractive Processes in Photoproduction and DIS.", in Proc. of the Europhysics Conference, Marseilles, France, July 1993, ed. J. Carr and M. Perrottet, p. 585.
J. B. Dainton, "Results from the H1 Experiment at HERA.", in Proc. XVI International Symposium on Lepton Photon Interactions, Cornell, Ithaca, USA, August 1993, ed. P. Drell and D. Rubin, p. 87 and Rutherford Appleton Laboratory preprint RAL 94-12.
A. De Roeck, "Results from the H1 Experiment.", in Proc. of the Europhysics Conference, Marseilles, France, July 1993, ed. J. Carr and M. Perrottet, p. 791 and DESY preprint DESY 94-005 (1994).
[48] T. Ahmed et al. (H1 Collaboration), Nucl. Phys. **B429** (1994) 477.
[49] see for example J. Ellis, in Proc. "Study of an ep Facility for Europe", ed. U. Amaldi, DESY 79-48 (1979).
[50] R. P. Feynman, "Photon Hadron Interactions", 1972, W. Benjamin Inc., **ISBN 0–805–32510–7**, p. 344.
[51] J. D. Bjorken, "Hard Diffraction and Deep–Inelastic Scattering", in Proc. Int. Workshop on Deep–Inelastic Scattering and Related Topics, Eilat, Israel, 1994, ed. Aharon Levy, World Scientific, **ISBN 981–02–2053–7**, p. 151, and earlier references therein.
[52] G. Ingelman and K. Janson–Prytz, "The Pomeron Structure Function and QCD at Small–x", in Proceedings of the Workshop "Physics at HERA", p. 233, October 1991, ed. W. Buchmüller and G. Ingelman.
[53] G. Ingelman and K. Prytz, Zeit. Phys. **C58** (1993) 285.
[54] T. Ahmed et al. (H1 Collaboration), Phys. Lett. **B348** (1995) 681.
[55] H. Jung, Comput. Phys. Commun. **86** (1995) 147.
[56] T. Regge, Nuov. Cim. **14** (1959) 951, Nuov. Cim. **18** (1960) 947.
[57] G. Chew, S. Frautschi, S. Mandelstam, Phys. Rev. **126** (1962) 1202.
[58] P. Collins and E. Squires, "An Introduction to Regge Theory and High Energy Physics", Cambridge University Press, Cambridge (1977).
[59] A. Donnachie and P. Landshoff, Nucl. Phys. **B303** (1988) 634.
[60] L. N. Lipatov, Sov. Phys. JETP **63** (1986) 904.
[61] M. Genovese, N. N. Nikolaev, B. G. Zakharov, "Diffractive DIS from the generalised BFKL pomeron. Predictions for HERA.", Institut für Kernphysik, KFA, Jülich preprint KFA–IKP(Th)–1994–37.
[62] C. Pascaud, F. Zomer, LAL preprint LAL/94-42.
[63] J. P. Phillips, "Rapidity Gap Events at HERA and the Structure of the Pomeron", these proceedings.
[64] E. Witten, Nucl. Phys. **B120** (1977) 189.
[65] W. Buchmüller, A. Hebecker, "A Parton Model for Diffractive Processes in Deep–Inelastic Scattering", DESY preprint DESY 95–077 (1995).
[66] J. Bartels, in a presentation at the Int. Workshop on Deep–Inelastic Scattering and Related Topics, Eilat, Israel, February 1994 (Proceedings ed. Aharon Levy, World Scientific, **ISBN 981–02–2053–7**).
[67] S. Aid et al. (H1 Collaboration), "Measurement of the e+ and e- induced charged current cross sections at HERA", DESY-95-102, to appear in Zeit. Phys.
[68] S. Aid et al. (H1 Collaboration), Phys. Lett. **B353** (1995) 578.